MONTANA STATE UNIVERSITY

Resistivity and heat transfer characteristics of high temperature film anemometers
by Scott Gerald Anders

A thesis submitted in partial fulfillment of the requirements for the degree of Master of Science
Mechanical Engineering
Montana State University
© Copyright by Scott Gerald Anders (1990)

Abstract:
The resistivity and heat transfer characteristics of a wedge-shaped high temperature film anemometer probe are studied here. These film anemometers were designed specifically for flows with stagnation temperatures up to 760 C and dynamic pressures of around 20 psia. The necessary theory was first developed from low speed applications of film anemometers and from hot-wire theory. The proper calibration equipment and procedures were selected so that the required raw data could be collected. The theory was used to reduce the data to the variables of interest. Oven calibration data were taken for the temperature range 20 C to 500 C. The resulting data were fit with a second degree polynomial in order to give the correct reference resistance and resistivity coefficients which were unique for each probe. Flow data were taken for Mach numbers 0, 0.5, 1, 2, and 3. Data for Mach 0.5, 1, 2, and 3 were taken at stagnation temperatures of 15 C and 65 C. The resulting dimensional Reynolds number range covered by these various flows was from zero to 120,000 1/cm. Small amounts of data were also collected at Mach 6 and Mach 8. For the flows investigated the Nusselt number was found to be a function of the square root of the Reynolds number with no apparent Mach number dependence. In order to obtain this Nusselt number the measured Nusselt number must be corrected for its conduction contribution as the developed theory indicates. The temperature recovery factor was found to have a maximum at a value of approximately one and it was found to decrease with increasing Mach number to a minimum of about .8 at Mach 8. It also exhibited a Reynolds number dependence for Mach numbers of 3 and higher.

RESISTIVITY AND HEAT TRANSFER CHARACTERISTICS OF HIGH TEMPERATURE FILM ANEMOMETERS

by

Scott Gerald Anders

A thesis submitted in partial fulfillment
of the requirements for the degree

of

Master of Science

in

Mechanical Engineering

MONTANA STATE UNIVERSITY
Bozeman, Montana

May 1990

N378
An206

APPROVAL

of a thesis submitted by

Scott Gerald Anders

This thesis has been read by each member of the thesis committee and has been found to be satisfactory regarding content, English usage, format, citations, bibliographic style, and consistency, and is ready for submission to the College of Graduate Studies.

5/15/90
Date

Chairperson, Graduate Committee

Approved for the Major Department

5/15/90
Date

W. E. Larsen
Head, Major Department

Approved for the College of Graduate Studies

May 25, 1990
Date

Graduate Dean

STATEMENT OF PERMISSION TO USE

In presenting this thesis in partial fulfillment of the requirements for a master's degree at Montana State University, I agree that the Library shall make it available to borrowers under rules of the Library. Brief quotations from this thesis are allowable without special permission, provided that accurate acknowledgment of source is made.

Permission for extensive quotation from or reproduction of this thesis may be granted by my major professor, or in his absence, by the Dean of Libraries when, in the opinion of either, the proposed use of the material is for scholarly purposes. Any copying or use of the material in this thesis for financial gain shall not be allowed without my written permission.

Signature Scott D. Anders

Date 5/15/92

ACKNOWLEDGMENTS

The author is indebted to the following persons for their contributions to this investigation:

His advisor, Dr. Anthony Demetriades, for his guidance throughout this investigation.

John Rompel, for designing and constructing the special electronic equipment used in this investigation.

Pat Vowell, for his assistance in constructing or repairing the equipment used in this investigation.

Dr. Alan George and Dr. Richard Rosa for their support as committee members.

The Mechanical Engineering Department of Montana State University for financial assistance.

The Calspan Corporation, AEDC operations, for consultations regarding hot-film data.

Rene' Tritz, for typing and checking the final version of this thesis.

TABLE OF CONTENTS

TABLE OF CONTENTS—Continued

LIST OF TABLES

LIST OF FIGURES

LIST OF FIGURES—Continued

LIST OF FIGURES—Continued

LIST OF FIGURES—Continued

NOMENCLATURE

Symbol	Description
A	Cross sectional area
A_S	Surface area
c	Constant
d	Diameter
G	Grashof number
g	Gravitational constant
h	Convective heat transfer coefficient
i	Current
k	Thermal conductivity
L_C	Conduction loss term
l	Length of sensor
LVT	Low velocity tunnel
M	Mach number
N	Nusselt number
Ncnd	Conduction contribution to measured Nusselt number
Nm	Measured Nusselt number
P	Perimeter
PCS	Programmable Current Supply
Pr	Prandtl number

NOMENCLATURE–Continued

Symbol	Description
Qrad	Heat transfer due to radiation
q	Heat transfer rate
R	Resistance
R_C	Resistance of cable connecting probe to current supply
R_{LW}	Resistance of platinum wire leads
R_T	Total line resistance
Re	Reynolds number
r	Radius
SWT	Supersonic wind tunnel
T	Temperature
V	Velocity
W	Power
y	Differential height of manometer
α	First coefficient of resistivity
β	Second coefficient of resistivity
γ	Specific weight
ϵ	Emissivity
η	Temperature recovery factor
ξ	Third coefficient of resistivity
σ	Stefan-Boltzmann constant
τ	Temperature loading factor

NOMENCLATURE–Continued

Symbol	Description
$(\ )_e$	At recovery temperature
$(\ )_f$	Based on film
$(\ )_r$	At reference condition (0 C)
$(\ )_s$	At supports
$(\ )_w$	Based on wire
$(\ )_\infty$	At free-stream temperature

ABSTRACT

The resistivity and heat transfer characteristics of a wedge-shaped high temperature film anemometer probe are studied here. These film anemometers were designed specifically for flows with stagnation temperatures up to 760 C and dynamic pressures of around 20 psia. The necessary theory was first developed from low speed applications of film anemometers and from hot-wire theory. The proper calibration equipment and procedures were selected so that the required raw data could be collected. The theory was used to reduce the data to the variables of interest. Oven calibration data were taken for the temperature range 20 C to 500 C. The resulting data were fit with a second degree polynomial in order to give the correct reference resistance and resistivity coefficients which were unique for each probe. Flow data were taken for Mach numbers 0, 0.5, 1, 2, and 3. Data for Mach 0.5, 1, 2, and 3 were taken at stagnation temperatures of 15 C and 65 C. The resulting dimensional Reynolds number range covered by these various flows was from zero to 120,000 1/cm. Small amounts of data were also collected at Mach 6 and Mach 8. For the flows investigated the Nusselt number was found to be a function of the square root of the Reynolds number with no apparent Mach number dependence. In order to obtain this Nusselt number the measured Nusselt number must be corrected for its conduction contribution as the developed theory indicates. The temperature recovery factor was found to have a maximum at a value of approximately one and it was found to decrease with increasing Mach number to a minimum of about .8 at Mach 8. It also exhibited a Reynolds number dependence for Mach numbers of 3 and higher.

CHAPTER 1

INTRODUCTION

As the area of supersonic and hypersonic research expands, the need for improved instrumentation to measure both mean flow properties and turbulent fluctuations becomes increasingly important. The majority of information in the area of turbulence fluctuation measurement has been gathered by the hot-wire anemometer. The hot-wire consists of a very fine wire mounted perpendicular to the flow on two small supports. By monitoring the resistance and power dissipation of the wire, the recovery temperature and the Nusselt number can be determined. If these are then investigated for different flow regimes their dependence on Mach number, Reynolds number, and temperature can be determined. These dependencies can then be used in the measurement of turbulent fluctuations. Further discussion on the hot-wire method can be found in References [1-4].

Though hot-wires have proven themselves useful, they are limited to flows where the temperatures and dynamic pressures are moderate. They also retain some undesirable characteristics such as a Mach number dependence at low Reynolds numbers due to restrictions on spatial resolution. Since high Mach number and high dynamic pressure facilities are usually small in order to be economically justifiable, the areas of interest in a particular flow to be studied require instrumentation that has high spatial resolution. A high spatial resolution is also

required if high turbulence frequencies (responses of around 300 kHz) are going to be measured. These requirements in turn put limitations on the magnitude of hot-wire diameters. These small diameter wires bring the instrument into the low Reynolds number range where the Nusselt number becomes Mach number dependent. Also, when flow dynamic pressures or stagnation temperatures become high the mechanical strength of the hot-wire is found insufficient to prevent wire breakage. To make the situation even more severe, many facilities are not adequately filtered to remove tiny particles which can destroy the small unsupported wire. These requirements for a high structural endurance, high frequency response, and high spatial resolution have given rise to the film anemometer probe.

Film anemometer probes have been used in the past mainly for measurement in liquids such as water and blood where hot-wires would be impractical [2,5,6]. The use of a film anemometer probe in a supersonic flow has received limited attention however, resulting in limited sources on their calibration methods, resistivity, and heat transfer characteristics. Now that more severe requirements have been placed on this type of instrumentation, use of the film anemometer has become more promising and the need for knowing its characteristics increasingly important. The requirements for the film anemometer probes investigated here were that the probes must be able to be used for high temperature (760 C), high dynamic pressure flows [7]. For these probes, the films are deposited on the stagnation line of a wedge-shaped probe tip. This film, being supported by the hard probe body tip, is much less subject to failure due to mechanical stresses as compared to the hot-wire yet still will be able to maintain the required frequency response and spatial resolution.

The theory developed for the films is drawn from low speed applications of film anemometers and from hot-wire anemometer theory which shares many points of

similarity. Much of the theory has also been previously established by Ling [8] and Demetriades [7]. The calibration methods used here are developed on the basis of this theory, the results of which show that the heat transfer characteristics of hot-films are quite similar to hot-wires. The most noticeable deviation is the large conduction loss to the substrate for the film.

Much time was spent investigating the hot-film probe resistivity and heat transfer characteristics since they must be understood in order to move on to the measurement of turbulence fluctuations. In order to make proper measurement of turbulence one must know accurately: the resistance and resistivity coefficients; the temperature recovery factor dependence on Mach number, stagnation temperature, Reynolds number; and the Nusselt number dependence on Mach number, stagnation temperature, Reynolds number, and temperature loading (power). The following is an account of how all of these are determined and the results of each. For information on the use of these characteristics for turbulent flow measurements see Demetriades [9].

CHAPTER 2

FILM ANEMOMETER PRINCIPLE AND RESEARCH GOALS

The principle of operation of the hot-film anemometer probe is the following: If an object is placed in a moving medium and then heated, heat will be exchanged between the object and the medium. The rate at which the heat is exchanged depends on the characteristics of the object, the physical characteristics of the medium, and the flow characteristics of the medium. The heat is introduced by a constant electrical current and the corresponding resistance of the object is monitored. By first observing and recording the behavior of the object for a variety of flow conditions, the object can later be used to determine unknown flow characteristics. This is the general method described and used by Laufer and McClellan [10].

The two aims of this research were to determine (a) the resistivity characteristics and (b) the heat transfer characteristics for film anemometers designed for high temperature hypersonic research. These film anemometers were designed to be able to withstand continuous exposure to 760 C stagnation temperatures and dynamic pressure loads exceeding 140 kPa (20 psia). This placed serious restrictions on probe design and development. Despite the design problems the two aims of this research were carried out while the probes were being developed. The determination of the resistance and resistivity characteristics included selection of the proper calibration equipment and procedures and the determination of the proper handling of the calibration data. The determination of the heat transfer

characteristics of the film anemometer probe also included selection of the proper calibration equipment, procedures and data handling. In addition to these the second aim included determination of the proper theory of measurement, relating the film anemometer probe electrical output to flow dependence variables by theory, and relating these variables to the flow characteristics such as the temperature recovery factor, Reynolds number, Mach number, and flow temperature.

CHAPTER 3

HEAT BALANCE FOR THERMAL SENSORS

As briefly mentioned in Chapter 2, the rate at which heat is exchanged from the object to the medium depends on the characteristics of the object, the physical characteristics of the medium, and the flow characteristics of the medium. In order to measure these flow characteristics by the method described, the rate at which heat is exchanged to the medium must be known. This requires analysis of the heat loss for the object of interest. The approach taken here is to start with the simplest model and work towards the desired but more complicated model.

Cylinder With No Conduction Loss

An electrically heated cylinder in a cross flow with no end losses can lose heat only by radiation and convection. If it is assumed that radiation losses are negligible the power balance is

$$i^2 R = h A_S (T - T_\infty) \tag{1}$$

where

$i^2 R$ = power input

h = convective heat transfer coefficient

A_S = surface area

T = temperature of film

T_∞ = temperature of surroundings .

See pages xii–xiv for list of nomenclature used throughout the text. For a cylinder immersed in a compressible flow the temperature of the fluid nearest the sensor will not be the free stream stagnation temperature but instead some fraction of that temperature. In order to better satisfy the physics of the situation, (1) will be rewritten as

$$i^2 R = h 2\pi r \ell (T - T_e) \quad . \tag{2}$$

The recovery temperature, T_e, is the temperature of the wire at zero current. In terms of the Nusselt number, (2) is

$$i^2 R = \pi \ell k_e N (T - T_e) \quad . \tag{3}$$

Again by arguments of the physical situation the thermal conductivity, k_e, is based on the recovery temperature.

Cylinder With Conduction Loss

For the above situation with added conduction losses, the form of the equation remains approximately the same by the following argument developed by Demetriades [7]. The heat balance is now

$$i^2 R = \pi \ell k_e N (T - T_e) + L_C \quad . \tag{4}$$

The added conduction loss term, L_C, must be roughly proportional to the thermal conductivity of the wire, k_w, the temperature difference between the wire and the support, $(T - T_S)$, and the wire cross sectional area. It must also be roughly inversely proportional to the length, ℓ, of the wire. Combining these arguments gives

$$L_C = C_1 \frac{\pi d^2 k_w}{4\ell} (T - T_S) \quad , \quad C_1 = \text{constant} \quad . \tag{5}$$

Since the supports are many times larger than the wire and are wetted by the flow at temperature T_e, the supports can be assumed to be approximately at the recovery temperature also (lack of knowing the actual temperature leads the experimentalist to make some kind of assumption and the one assumed here is as appropriate as any). Equation (4) can now be written as

$$i^2 R = \pi \ell k_e N (T - T_e) + C_1 \frac{\pi d^2 k_w}{4\ell} (T - T_e) \quad . \tag{6}$$

This new conduction term can now be absorbed into a new Nusselt number which will include both conduction and convection losses so that

$$i^2 R = \pi \ell k_e Nm (T - T_e) \tag{7}$$

where

$$Nm = N + \left(\frac{d^2}{\ell^2} \frac{C_1}{4} \frac{k_w}{k_e} \right) \tag{8}$$

or

$$Nm = N \left(1 + \frac{C}{S^2} \right) \quad , \quad S^2 = \frac{\ell^2}{d^2} \frac{k_e}{k_w} N \quad . \tag{9}$$

If the term appearing in parenthesis in (8) or (9) is large then the conduction term is significant.

Kovasznay [11] and Dewey [12] have performed a more detailed calculation of the end losses. Their results are

$$Nm = N/\psi(S) \tag{10}$$

where $\psi(S)$ is the correction. The dimensional argument indicates that S depends on the Nusselt number and the temperature loading. Therefore (10) can be written as

$$Nm = \frac{N}{f(N, \tau)} = Nm(N, \tau) \tag{11}$$

or

$$i^2 R = \pi \ell k_e N m(N,\tau)(T - T_e) \quad . \tag{12}$$

Kovasznay [11] and Dewey [12] give the exact solution as

$$\psi(S) = 1 - \frac{\tanh S}{S} \quad . \tag{13}$$

By comparing the exact solution given by (13) to the approximate solution given by (9) Demetriades [7] gives

$$\psi(S) = \frac{1}{1 + \frac{C}{S^2}} \quad . \tag{14}$$

This is satisfactorily close to (13) if the constant C is about four according to Demetriades [7].

Film Anemometer With No Substrate

For an electrically heated film with negligible radiation losses (see Appendix A) and no conduction losses the heat balance is

$$i^2 R = h A_S (T - T_e) \tag{15}$$

or, in terms of the Nusselt number,

$$i^2 R = k_e N A_S / w (T - T_e) \quad . \tag{16}$$

For the "homemade" films used, the area and characteristic length are not physically defined well enough to measure with acceptable accuracy. To accommodate this difficulty a new dimensional Nusselt number is defined as

$$N' = N A_S / w \tag{17}$$

so that (16) is now

$$i^2 R = k_e N'(T - T_e) \quad . \tag{18}$$

Film Anemometer With Substrate

Assuming that the heat balance equation is of the same form as (18), the heat balance can be written

$$i^2 R = k_e N'(T - T_e) + L_C \quad . \tag{19}$$

Using the same argument as that used for the wire the conduction loss can be written as

$$L_C = C k_S \frac{A_S}{L} (T - T_e) \quad . \tag{20}$$

Yet another Nusselt number will be defined that is dimensional and includes both conduction and convection losses as

$$Nm' = N' + C_1 \frac{k_S}{k_e} \frac{A_S}{L} \quad . \tag{21}$$

Equation (19) can now be written in the form of convection losses only as shown in the following equation:

$$i^2 R = k_e Nm'(T - T_e) \quad . \tag{22}$$

It is known analytically and experimentally that the heat loss due to conduction to the supports is quite small for wires. Experimental results have shown that this is not so for films. In order to look more closely at this heat loss, a "thin-rod" model of the heat loss to the substrate will be examined. Figure 1

shows this model. This model assumes a constant cross sectional area and a constant thermal conductivity. It also assumes that the only temperature gradient is along the axis (no radial temperature distribution), that the face is held at a constant temperature, that the cylinder approaches the surrounding temperature as it extends to infinity, and that the surrounding temperature is the recovery temperature of the film. The differential equation describing the heat loss is

$$\frac{d^2T}{dx^2} - \frac{h_B P}{k_S A}(T - T_e) = 0 \tag{23}$$

where

h_B = heat transfer coefficient for probe body

P = perimeter of probe body

k_S = thermal conductivity of substrate

A = body cross sectional area .

Solving this equation gives the temperature distribution as

$$T = T_e + (T_f - T_e)e^{-\sqrt{\frac{h_B P}{k_S A}}\,x} \quad . \tag{24}$$

For a circular rod this may be written as

$$T = T_e + (T_f - T_e)e^{-\sqrt{\frac{2h_B}{k_S r}}\,x} \quad . \tag{25}$$

From (25) L in (21) can be approximated by taking the slope at $x = 0$ of (25) and extending a line formed by this slope to the point where the temperature is equal to the fluid temperature as in Figure 2. If this is done it is found that

$$L = \sqrt{\frac{k_S r}{2h_B}} \tag{26}$$

or in terms of the Nusselt number of the rod near the film

$$L = r\sqrt{\frac{k_S}{k_e}\,\frac{1}{2N_B}} \quad . \tag{27}$$

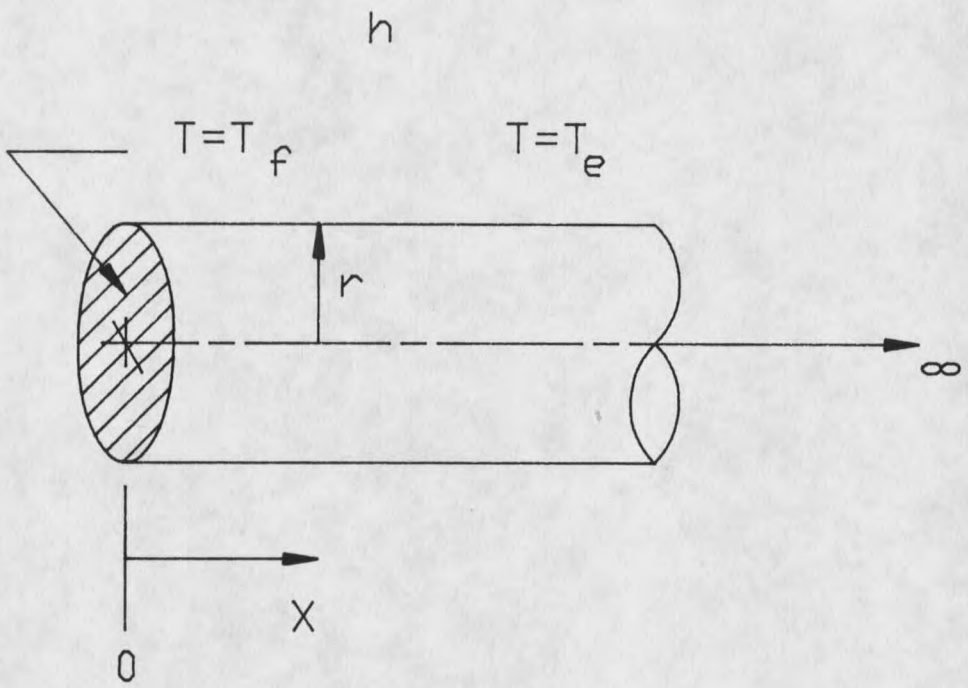

B.C.

At $x=0$ $\quad T=T_f$

As $x \to \infty$ $T \to T_e$

A = constant

k_s = constant

Figure 1. One-Dimensional Model for Heat Loss to Substrate.

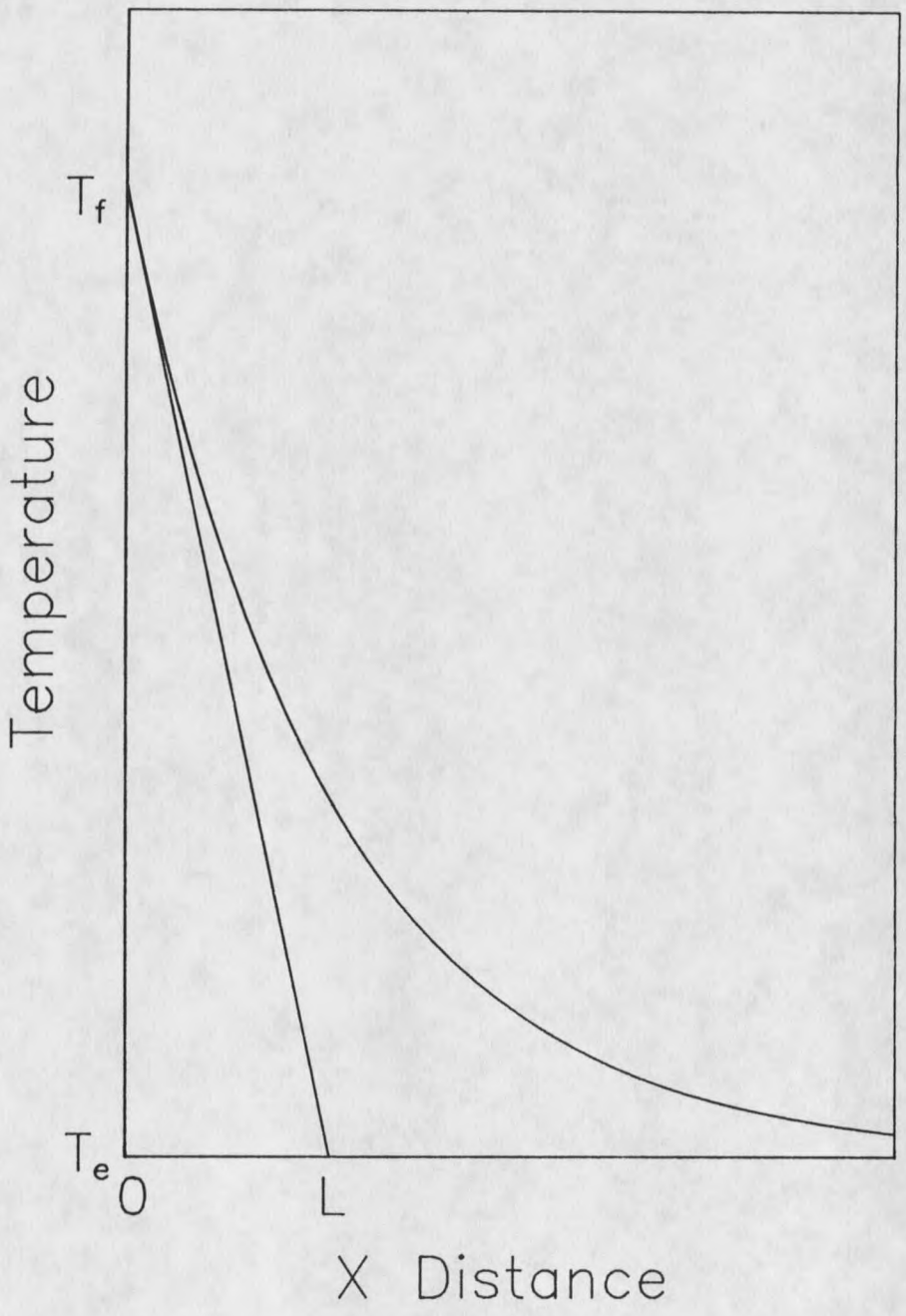

Figure 2. Approximation of Distance L for "Thin-Rod" Model.

Substituting (27) into (21) gives

$$Nm' = N' + C_1 \frac{A_f}{r}\sqrt{\frac{k_S}{k_e}\,2N_B} \quad . \tag{28}$$

This equation says that for a low conduction loss the thermal conductivity of the substrate must be minimized. It can also be seen that since the thermal conductivity of the air is temperature dependent, the conduction loss term will also be temperature dependent. The thermal conductivity of the substrate material may also be temperature dependent. This dependence can not easily be found since the substrate can come in a truly infinite number of compositions and therefore tabulated data is likely unavailable. It is known by looking at [13] that some glasses vary as much as 10% in conductivity in the temperature range from zero to 100 C and that the amount by which the thermal conductivity changes will depend on the particular temperature range investigated. All other terms in (28) affect the convection loss as well as the conduction loss. The magnitude of these effects cannot be determined easily theoretically. It is known experimentally that this conduction loss term can amount to over 50% of the magnitude of the measured Nusselt number, Nm', for Reynolds numbers ranging up to 100,000 1/cm.

Unfortunately the variable found from experiment is the measured Nusselt number, Nm', in (28) which is dimensional and includes conduction effects. The variable of interest however is the convective Nusselt number, N. In order to extract this variable from the measured quantity additional work has to be done when reducing the data. This will be described later in Chapter 4.

General Heat Balance Equation

Regardless of the sensors examined or the boundary conditions applied, all of the heat balance equations developed so far have had the same general form. By

examining equations (3), (7), (18) and (22) it can be seen that the general form is

$$i^2 R = k_e \overline{N}(T - T_e) \tag{29}$$

where $\overline{N}$ may include dimensions or conduction losses and is a function of Mach number, Reynolds number, and Temperature Loading (power). For films, $\overline{N}$, is dimensional and includes conduction losses. This general heat balance equation was originally noted by Demetriades [7].

CHAPTER 4

THEORY OF MEASUREMENT

From the theory of heat transfer from a film anemometer, the measured Nusselt number can be found by (22):

$$Nm' = \frac{i^2 R}{k_e(T - T_e)} \quad . \tag{30}$$

This expression is not nearly as simple as it first appears. The Nusselt number cannot be determined for the following reasons:

1. The recovery temperature, T_e, is not known.
2. Since the thermal conductivity is a function of the recovery temperature it is also an unknown.
3. The value of the measured Nusselt number, Nm', is known through experimental work to be a function of power.
4. The Nusselt number found includes both convection and conduction effects (it is desired to find the "real" Nusselt number which includes convection effects only).

Resistance-Temperature Relations

In order to determine the recovery temperature, a relation between the resistance of the film and the surrounding temperature must be known. It is known that (reference [14]) resistance type sensors can be described by

$$R = R_r \left(1 + \alpha(T - T_r) + \beta(T - T_r)^2 + \xi(T - T_r)^3 + \cdots\right) \quad . \tag{31}$$

For the film anemometer probes studied for the targeted temperature range this equation does not include terms past the quadratic. The number of terms retained is effected by the operation range of the instrument and its physical properties. For instance, hot-wires were typically operated from 10–200 C and used a linear fit but the films here were targeted for 10–760 C where a linear fit was found inadequate, as will be shown in Chapter 8. This will give the resistance at the recovery temperature as

$$R_e = R_r \left(1 + \alpha(T_e - T_r) + \beta(T_e - T_r)^2\right) \quad . \tag{32}$$

The recovery temperature can now be found if the reference resistance, R_r, the resistivity coefficients, α and β, and the resistance at zero current, R_e, in the above equation are known. The equation will yield two solutions for the recovery temperature, only one of which will make sense physically. From (32) the recovery temperature is

$$T_e = \frac{-\alpha + \sqrt{\alpha^2 + 4\beta(R_e/R_r - 1)}}{2\beta} + T_r \quad . \tag{33}$$

As mentioned above, in order to determine the recovery temperature the reference resistance and the resistivity coefficients, α and β, must be determined. This is done by performing an "oven calibration". This calibration is done by finding the resistance at zero current for each known film temperature over a range of temperatures (see Chapter 7 for further detail on oven calibration procedures). The resulting set of resistance-temperature points can then be approximated by a second degree polynomial to obtain the coefficients in (32). Making the measurements of this needed resistance at zero current for each known temperature requires additional procedures. Points must be collected over a range of different powers and the resulting resistance versus power data fit to a second degree

polynomial as in Figure 3. This fit is then used to extrapolate to zero power to find the resistance at zero current. A second degree polynomial fit is chosen as the correct form of the relation by examining the theory of the dependence of the measured Nusselt number on power and by previous experimental results, as will be shown next.

Nusselt Number Dependence On Power

The dependence of the measured Nusselt number on power cannot be determined directly from theory but it is known that such a dependence exists by looking at past experimental work. A simple relation will be assumed by expanding one over the measured Nusselt number in a Taylor series expansion and retaining only the first two terms, which is sufficient according to Demetriades [7]:

$$\frac{1}{Nm'} = \frac{1}{Nm'_e} - \frac{1}{Nm'^2_e}\left(\frac{\partial Nm'}{\partial W}\right)_e W \quad ; \quad \left(\frac{\partial Nm'}{\partial W}\right)_e = \text{constant} \quad . \tag{34}$$

After manipulation of (30), (32), and (34) and then letting the reference temperature be 0 C it can be found that

$$\begin{aligned} R = R_e &+ W\left[\frac{\alpha R_r}{k_e Nm'_e} + \frac{R_r 2\beta T_e}{k_e Nm'_e}\right] \\ &- CW^2\left[\frac{\alpha R_r}{k_e Nm'_e} + \frac{R_r 2\beta T_e}{k_e Nm'_e} - \frac{R_r \beta}{Ck_e^2 Nm'^2_e}\right] \\ &- C^2W^3\left[\frac{R_r \beta 2}{Ck_e^2 Nm'^2_e}\right] + C_3W^4\left[\frac{R_r \beta}{k_e^2 CNm'^2_e}\right] \end{aligned} \tag{35}$$

where

$$C = \frac{1}{Nm'_e}\left(\frac{\partial Nm'}{\partial W}\right)_e \quad . \tag{36}$$

Equation (35) is in the following form:

$$R = R_e + AW + BW^2 + EW^3 + FW^4 \quad . \tag{37}$$

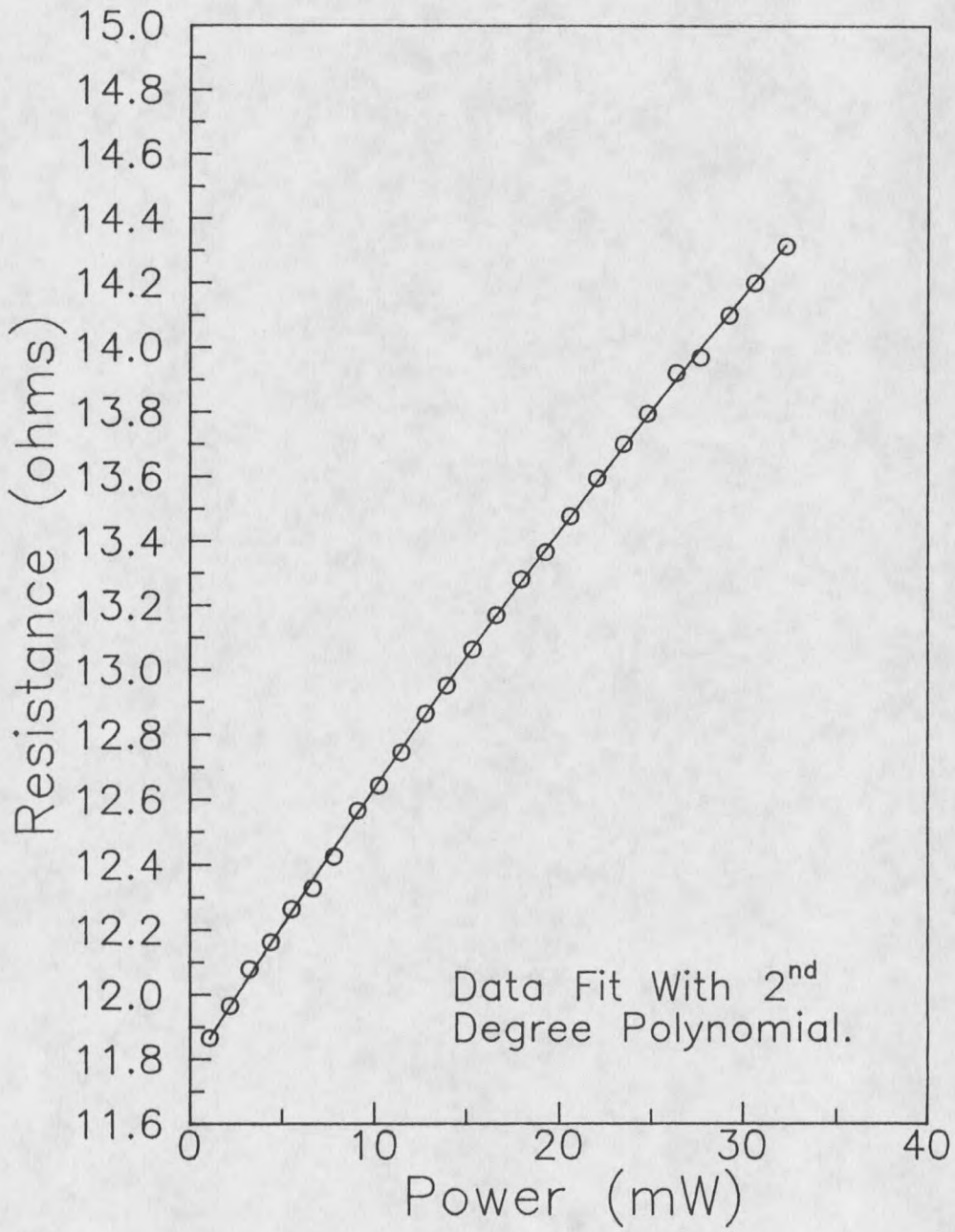

Figure 3. Film Resistance Dependence on Power Fit with a Second Degree Polynomial.

Equations (35) and (37) indicate that if the resistance versus power data are fit to a fourth order polynomial the measured Nusselt number at zero current can be found by relating the constant A in (37) to the corresponding term in (35) so that

$$Nm'_e = \frac{\alpha R_r}{Ak_e}\left(1 + \frac{2\beta T_e}{\alpha}\right) \quad . \tag{38}$$

However, it is known experimentally that the coefficients E and F in (37) are close to zero, making a second degree polynomial fit sufficient. In (38) all variables can now be determined. The recovery temperature is now known from (33). The thermal conductivity can be found knowing the recovery temperature by using a textbook relation such as found in Irvine and Liley [15]. The resistivity coefficients and the reference resistance can be found by performing an oven calibration and finally, by making a second degree fit of the power versus resistance data the variable A can be determined. This will give the measured Nusselt number at zero current which still needs to be corrected so that the Nusselt number which is controlled only by convection can be found.

The Nusselt number dependence on power can more easily be examined if (35) is put in non-dimensional form. Since the coefficients E and F are zero, (35) can be written more simply as

$$\begin{aligned} R = R_e + W\left[\frac{\alpha R_r}{k_e Nm'_e} + \frac{R_r 2\beta T_e}{k_e Nm'_e}\right] \\ + CW^2\left[\frac{\alpha R_r}{k_e Nm'_e} + \frac{R_r 2\beta T_e}{k_e Nm'_e} - \frac{R_r \beta}{Ck_e^2 Nm'^2_e}\right] \quad . \end{aligned} \tag{39}$$

Rewriting (39) in the form of (37) gives

$$R = R_e + AW + BW^2 \tag{40}$$

where

$$B = C\left[\frac{\alpha R_r}{k_e Nm'_e} + \frac{R_r^2 \beta T_e}{k_e Nm'_e} - \frac{R_r \beta}{Ck_e^2 Nm'^2_e}\right] \quad . \tag{41}$$

Now let

(42) $$G = \frac{B}{C}$$

and

(43) $$r = \frac{R - R_e}{R_e} \quad .$$

Substituting the above three equations into (39) will yield

(44) $$r = \frac{AW}{R_e} + \frac{A^2}{A^2}\,\frac{R_e}{R_e}\,B\,\frac{W^2}{R_e} \quad .$$

Let

(45) $$i_C^2 = 1/A$$

and

(46) $$w = W/W_C \quad ; \quad W_C = i_C^2 R_e$$

so that

(47) $$r = w - \frac{BR_e}{A^2}\,w^2 = w - \frac{CGR_e}{A^2}\,w^2 \quad .$$

Substitute (36) into (47):

(48) $$r = w - \frac{G}{A^2}\,R_e\,\frac{1}{Nm'_e}\left(\frac{2Nm'}{2W}\right)_e w^2 \quad .$$

Define a new variable D as

(49) $$D = \frac{G}{A^2}\,\frac{R_e}{Nm'_e} \quad .$$

Equation (48) is now written as

(50) $$r = w - Dw^2 \quad .$$

According to (49) the constant D indicates how the Nusselt number depends on power. This can more easily be seen if, for purposes of clarity, the effect of the β term (from the oven calibration) on the Nusselt number dependence on power is assumed to be negligible. This simplifies (49) to

$$D = \frac{k_e R_e}{\alpha R_r} \left(\frac{\partial N m'}{\partial W} \right)_e \quad . \tag{51}$$

Though (51) is not the true definition of the constant D it draws the same conclusion as (49) and can more easily be understood. By looking at (50) it can be seen that the constant D can simply be found by curve-fitting the non-dimensional power versus resistance points and extracting the second coefficient. The value of D found will indicate the dimensional Nusselt number dependence on power. A value of zero would indicate no dependence and a value different than zero would indicate the magnitude of the dependence. The variables w, r, and the constant D can also be used to determine if the number of terms in the Taylor Series expansion was sufficient by plotting $(1 - r/w)/D$ versus w. Demetriades [7] has done this and concluded that the number of terms retained in the expansion is sufficient.

Conduction Term Correction

The loss due to conduction should be able to be determined experimentally despite theoretical difficulties if it is assumed that the loss is solely a function of the thermal conductivity of the surrounding fluid (see (28)). By theory it was determined that the conduction contribution to the measured Nusselt number depends linearly on the inverse square root of the thermal conductivity of the surrounding fluid (see (28)).

Since the thermal conductivity is a function of temperature the conduction contribution can also be written as a function of temperature. This temperature dependent conduction contribution will show up in the measured Nusselt number versus Reynolds number data. Each set of data taken at a different stagnation temperature will lie on its own line as shown hypothetically in Figure 4 by the symbolic squares and circles on the graph. By taking the data found for the relation between the measured Nusselt number and Reynolds number for each set and extrapolating to zero Reynolds number a measured Nusselt number without a convection term can be found for that particular set of data (labeled as Ncnd1 and Ncnd2 on Figure 4). The resulting extrapolated value should approximately include only conduction losses. This method assumes that the Nusselt number will be zero at zero Reynolds number. This is not strictly true due to natural convection currents. Given a different extrapolated measured Nusselt number for each stagnation temperature over a range of temperatures, a relation that connects the conduction loss to the fluid temperature can be found. Each conduction loss can then be subtracted from its corresponding set of measured Nusselt number - Reynolds number points so that the resulting data would be as in Figure 5 where the Nusselt number is now the desired variable of interest. Unfortunately extensive Nusselt number - Reynolds number data may not be available, and were not available for the measurements made in this study, for a large number of different temperatures. The alternative solution would be to use the oven calibration data. For each point taken during the oven calibration there is a corresponding Nusselt number at that temperature. This can be estimated as the measured Nusselt number at zero Reynolds number (referred to as the extrapolated measured Nusselt number above) by neglecting convection currents (see Appendix B). Assuming the absence of convection and radiation leaves conduction to be the only contribution

to the measured Nusselt number in the enclosed oven chamber. By using the oven calibration data this way a relation that connects the conduction contribution of the measured Nusselt number to the surrounding temperature can be found. This conduction contribution can then be subtracted from the measured Nusselt number found in a flow so that the convection Nusselt number can be obtained, which is the desired parameter. The results of this procedure should be as shown in Figure 5.

Much effort has been expended in arriving at the convective Nusselt number. This Nusselt number is the variable through which the heat transfer characteristics will be studied, which is the desired point of investigation.

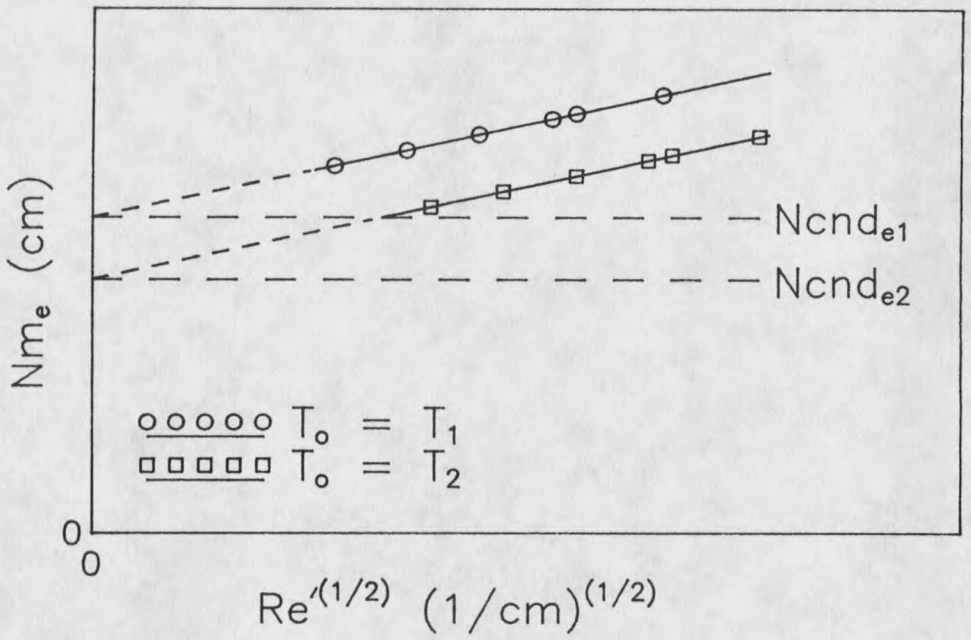

Figure 4. Hypothetical Case of Measured Nusselt Number Dependence on Flow Properties.

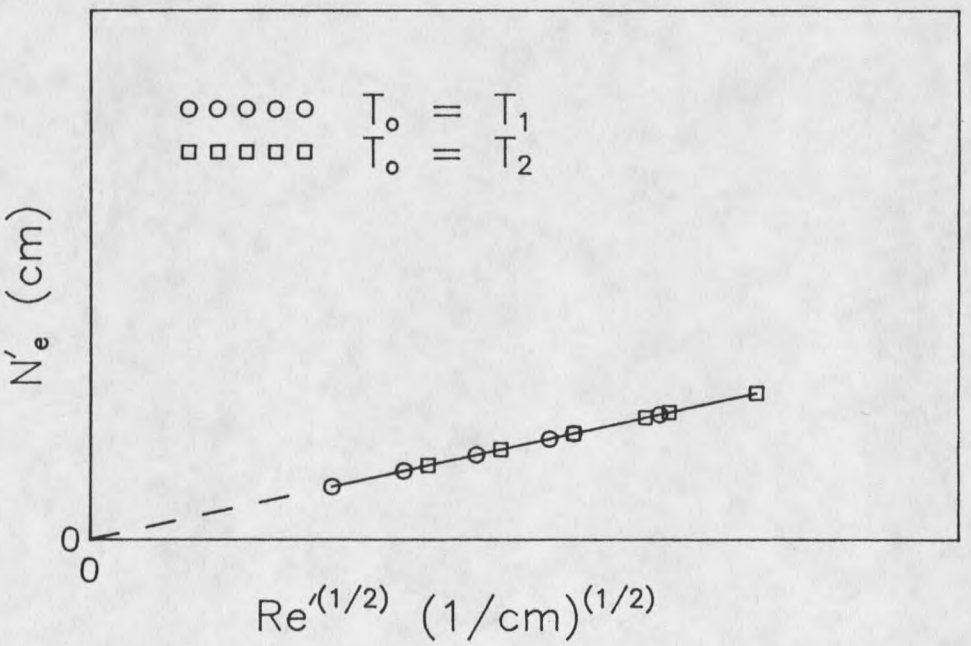

Figure 5. Hypothetical Case of "Actual" Nusselt Number Dependence on Flow Properties.

CHAPTER 5

HEAT TRANSFER FROM STAGNATION POINT SENSORS

Determining the Nusselt number is of no use unless it is somehow related to the flow characteristics. This is done by examining the heat transfer from stagnation point sensors and then drawing from hot-wire theory.

The local heat transfer rate of a sensor immersed in a flow is generally the highest at the stagnation line (Dewey [12], Sandborn [16], White [17]). Figure 6, originally presented by White [17], shows the local heat transfer rate from the surface of a hemisphere in a hypersonic laminar flow where $q_w(0)$ is the heat transfer at the stagnation line. The correlation shown agrees closely with experimental data [17]. Figure 6 clearly shows that the heat transfer rate is the greatest at the stagnation line as compared to the other positions investigated.

This conclusion can also be arrived at by examining the fact that the driving parameter for heat transfer is the temperature gradient between the heat transfer surface and the surrounding flow. This gradient depends heavily on the boundary layer thickness which is thinnest at the stagnation line, resulting in the highest gradient in this region [19]. Since a higher gradient results in a higher heat transfer rate one would expect that the heat transfer rate would be the greatest at the stagnation line.

From this conclusion it can be said that hot-wires exchange much of their total heat transferred at the stagnation line. Similarly, since films are deposited on the stagnation line, the film anemometer heat transfer theory should conform

closely with that of the hot-wire heat transfer theory; the theory which connects the Nusselt number to the various flow parameters such as the Reynolds number, Grashof number, Mach number, the temperature loading, etc. as follows [10]:

$$N = N(Re, M, G, Pr, \tau, \ldots) \quad . \tag{52}$$

Note that only forced convection is being considered. Also, for air in the range considered the Prandtl number will be taken as constant. This simplifies the above expression so that

$$N = N(Re, M, \tau) \quad . \tag{53}$$

This relation is shown by Dewey [12] in Figure 7. This figure indicates that the Nusselt number depends on Mach number for low Reynolds numbers where free-molecular effects are important [12]. From this and the previous conclusions regarding the similarities between film anemometers and hot-wires, film anemometers should follow the same general trends as found for hot-wires. The primary difference being that, since the hot-films are physically much larger than the hot-wires, the Reynolds number range shown in Figure 7 will be displaced to the right into the higher Reynolds number range for the hot-films. This would be of great advantage as it will eliminate the Mach number dependence of the Nusselt number on the Reynolds number. It is also expected that hot-films will show a Nusselt number dependence on the square root of the Reynolds number as is given by Kings Law [11] and as is found for hot-wires in the high Reynolds number range ($Re > 20$) ([12],[20]).

In addition to knowing the hot-wire and film Nusselt number dependence on the Reynolds number, it is also required to know the temperature recovery factor dependence on the Reynolds number before either instrument can be used

as a tool for measuring flow properties. Comparisons of hot-wires and hot-films are difficult here due to the effects of the different geometries and supporting methods of each type of sensor. It can only be predicted that the temperature recovery factor should be one at Mach number zero and remain fairly close to one (within about 10%) as the Mach number varies. Exact values can be found only by experiment since they will depend, at a minimum, on individual probe geometry and supporting method.

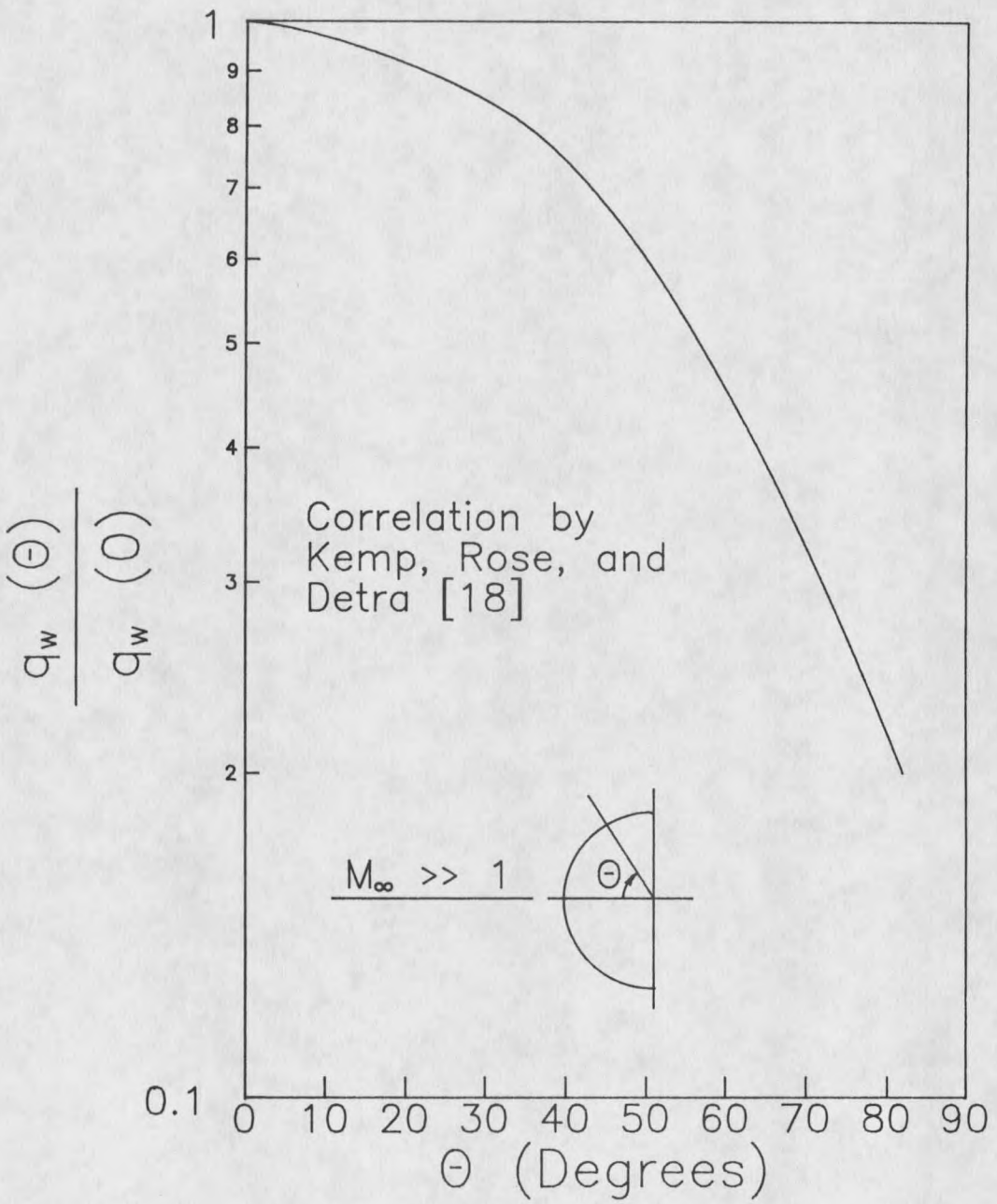

Figure 6. Local Heat Transfer Rate from the Surface of a Hemisphere in Hypersonic Flow.

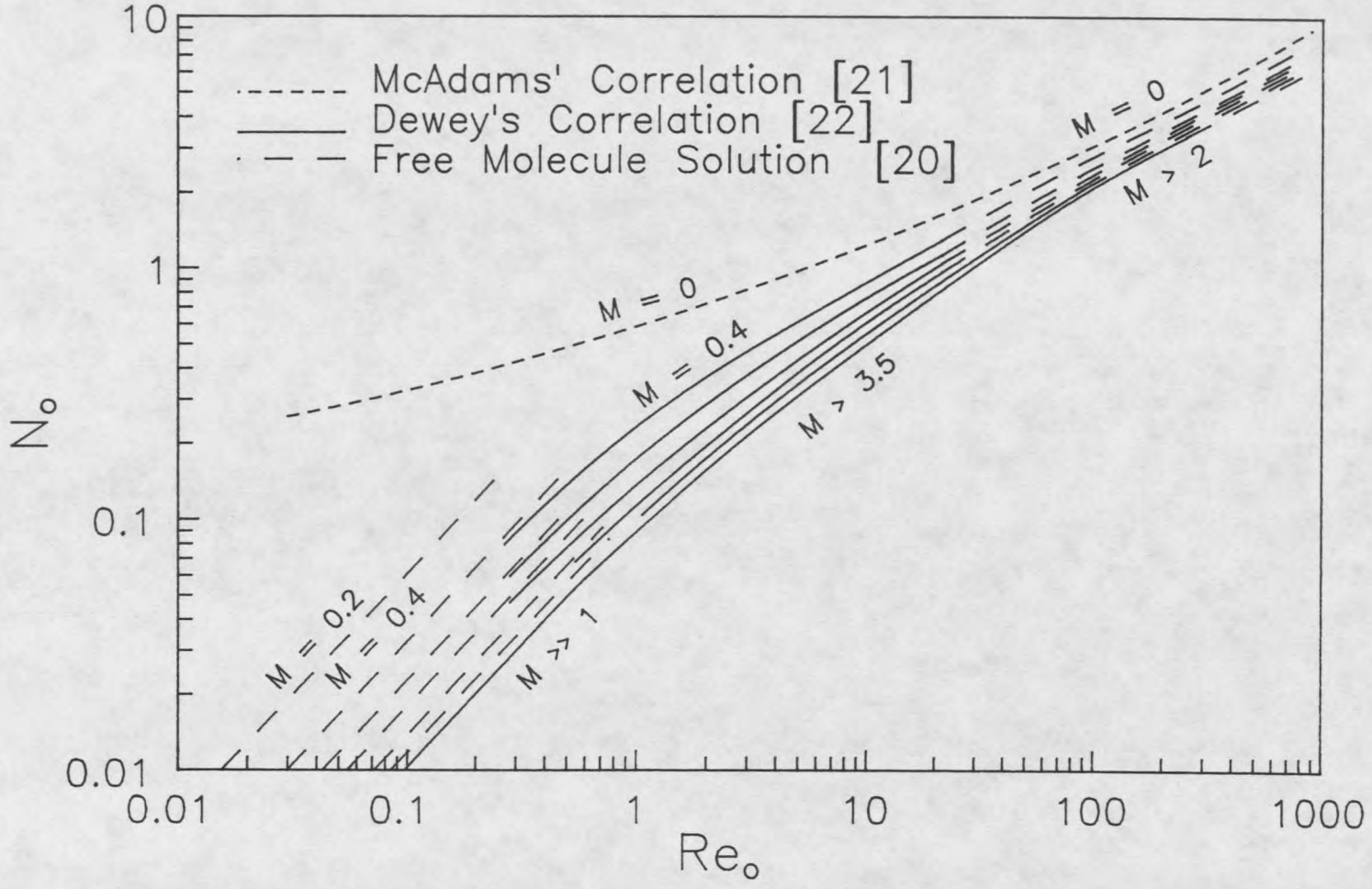

Figure 7. Correlation of Hot-Wire Heat Transfer at Low Reynolds Numbers. Nusselt and Reynolds Number Evaluated at Stagnation Temperature.

CHAPTER 6

EXPERIMENTAL APPARATUS

Film Anemometer Probes

The film anemometer probes studied were of the design shown in Figure 8. All of the hot-film probes studied were built at Montana State University by Dr. A. Demetriades. The probes were designed specifically for high temperature hypersonic flows. These particular flows are extremely restrictive for the probe design. The probes consist of four basic components which are the body, the leads, the glaze substrate, and the film. The main body is a 0.25 cm diameter 10 cm long twin-bore alumina tube. This was selected because it can easily withstand the temperature requirement and because of its availability. Two 24 gauge (0.05 cm diameter) 15 cm platinum lead wires extend through the alumina. These allow connection at one end to the electrical circuit and the other end to the film. Platinum was selected as the wire material since it is commercially available, is resistant to oxidation, and can withstand high temperatures. It is also chemically identical to the platinum film itself, resulting in a better film-leadwire joint. Possibly the most important component is the glaze substrate which supports the film. The glaze used was Amaco HF-10. A liquid platinum resinate was then used for the film. The film is deposited on the stagnation line of the probe tip and cured. The finished probes have resistances ranging from 5 to 25 ohms. The film area is about 0.18 cm by 0.05 cm and approximately .0000013 cm thick [9].

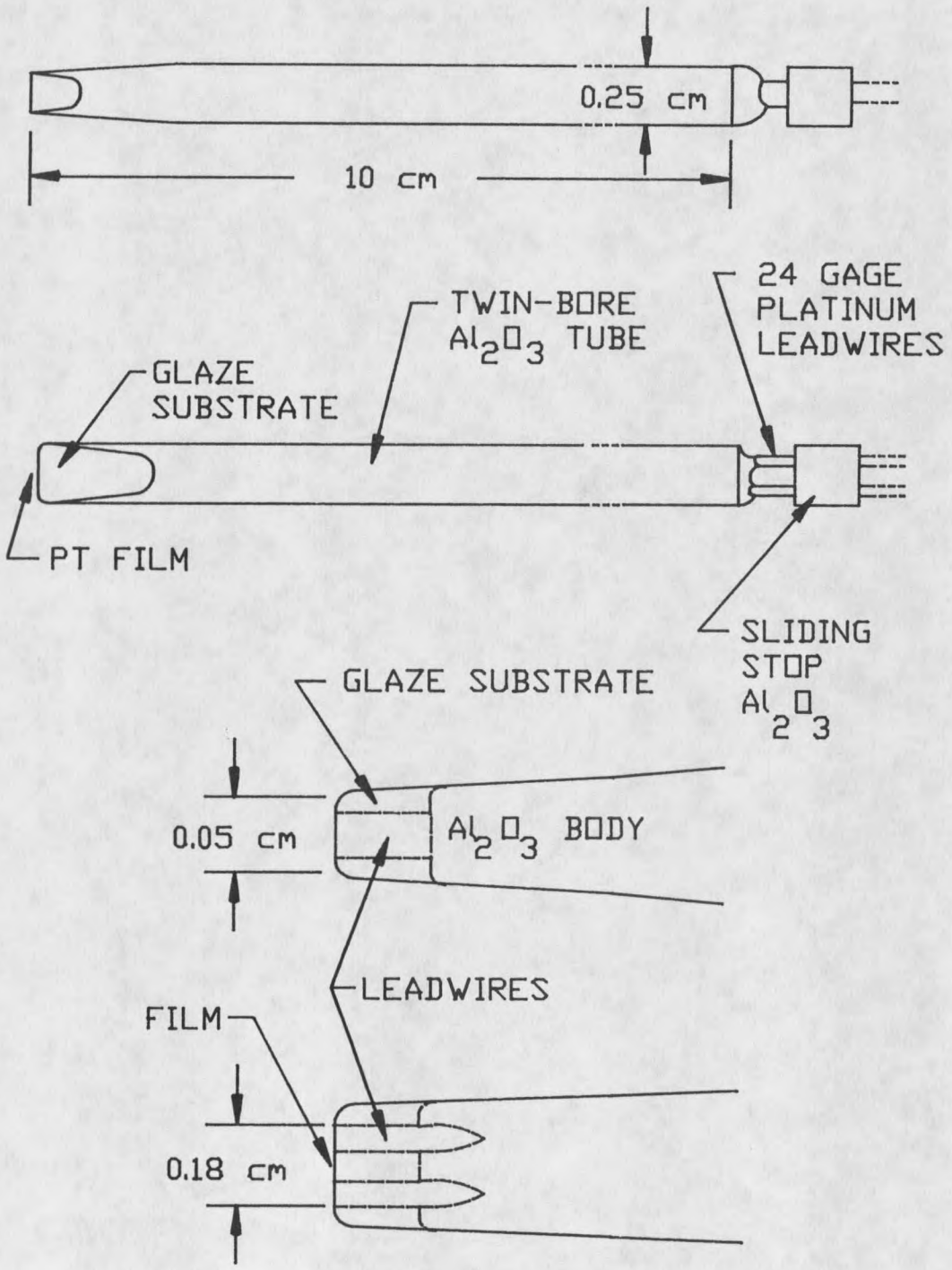

Figure 8. Film Probe Design.

As a part of the fabrication process the probes underwent preliminary tests consisting of stability checks at room temperature and high temperature soaks. For more information on the probe design and fabrication see [7].

Programmable Current Supply (PCS)

The electronic equipment used for making the necessary calibrations was a programmable current supply referred to as a PCS. The PCS is made up of a Zenith-100 microcomputer, a digital thermometer, and a computer controlled current supply. Figure 9 shows a diagram of the system components. The PCS is indispensable in making oven calibrations, flow calibrations, and single sets of current-increasing steps which will be referred to as "overheat traverses". The PCS allows several modes of operation ranging from manual to fully automatic. For example, for a single overheat traverse the PCS can be programmed to pass a specified number of sequential increasing currents through the film, stopping at a specified maximum current that can be up to 100 mA. Each temperature, voltage, current, and resistance is recorded by the computer. This data can then be stored in a data file for later data reduction. The PCS can also be programmed to monitor the temperature of the probe surroundings via a digital thermocouple and make overheat traverses at predetermined temperatures. By doing this the PCS can be set up to do complete oven calibrations without constant user supervision.

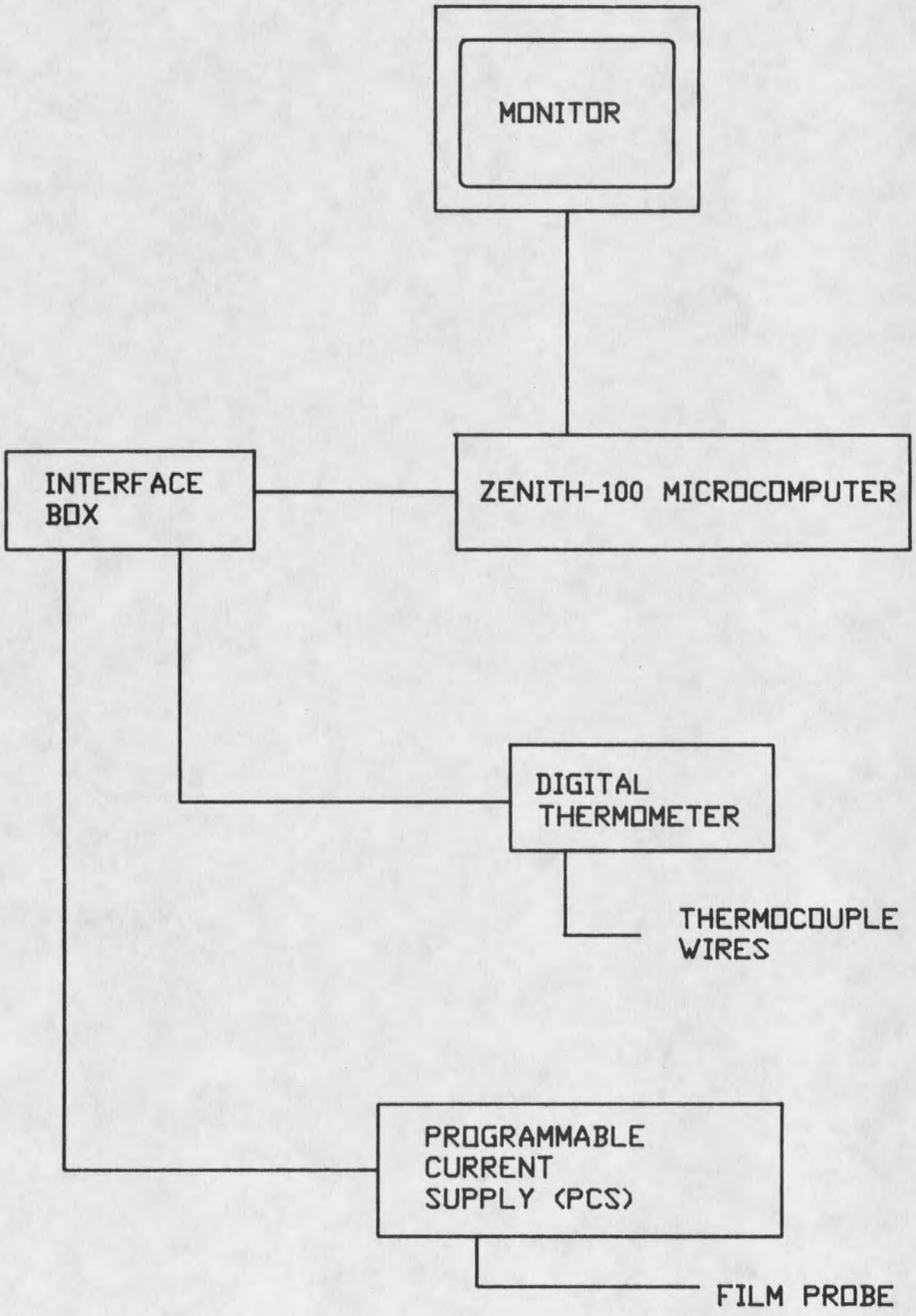

Figure 9. System Components Used to Collect Raw Data.

Oven Calibration Hardware

In order to find the reference resistance at 0 C and the resistivity coefficients for each probe, it is necessary to find the probe resistance at zero current for a range of temperatures. This must be done in a surrounding where the temperature can be measured accurately and independently of the film. This can be conveniently done by using a controlled oven. With the probe completely immersed in the oven with an accompanying thermocouple, the film temperature can be monitored. See Figure 10 for a schematic of the oven with the probe in place. Figure 11 shows the probe mounted in the oven probe holder. Once the probe is mounted on the holder and connected to the PCS the holder can be completely inserted into the oven chamber.

The oven is a Hevi-Duty Electronic Co. Model M-3012-S. It is a 30 cm outside diameter 45 cm long cylinder with a 5.7 cm diameter coaxially located insulated heating chamber lined with alumina. The heating chamber is accessible at one end by a sliding steel door. The probe holder is a ceramic plug which is made to slide completely into the heating chamber of the oven leaving only lead-wires and thermocouple leads protruding from a small opening in the door. The oven is rated at 1650 Watts and 1000 C. It is powered by a variable transformer with a 140 Volt maximum. The oven is capable of reaching 500 C in about 1 hour and cools to room temperature in about 12 hours.

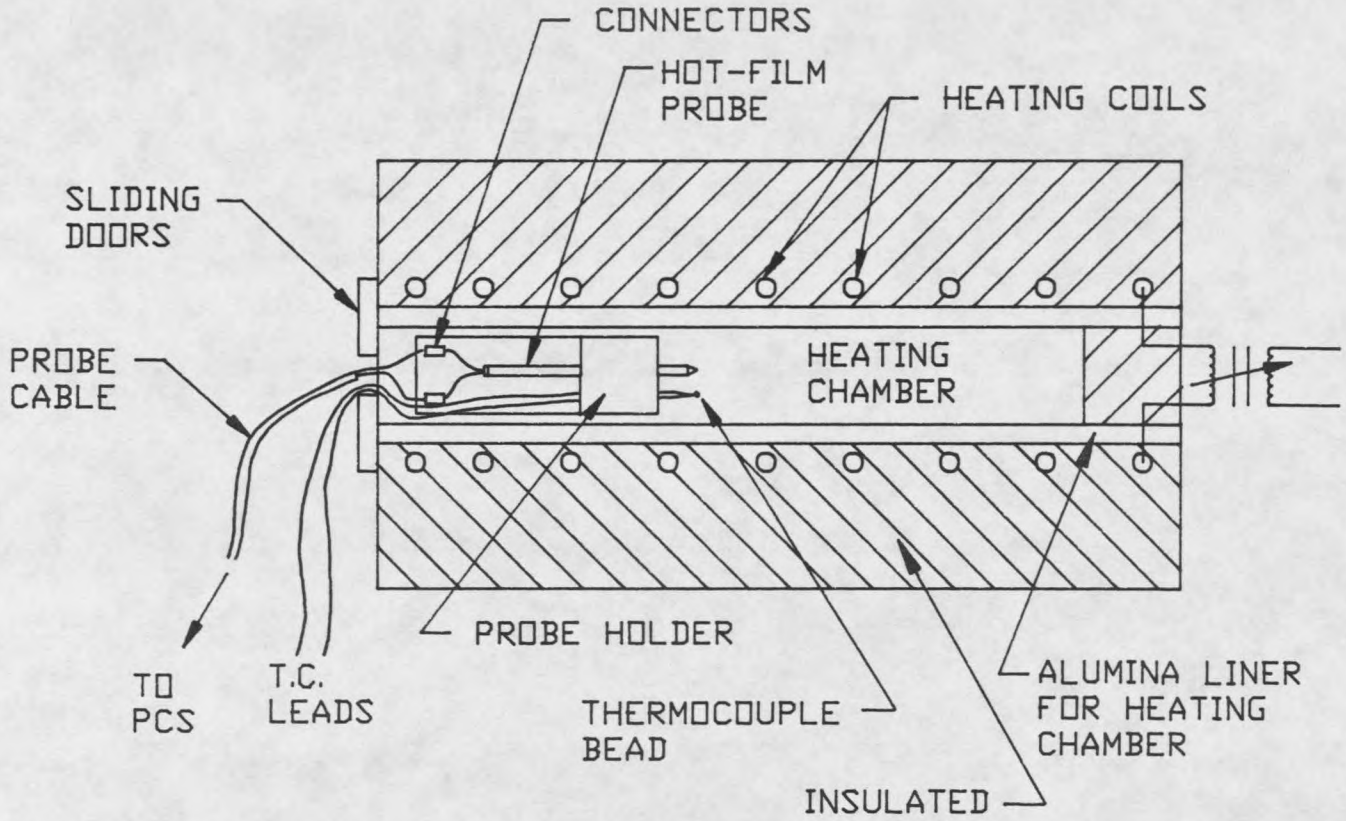

Figure 10. Top Cut-Away View of Oven Calibration Hardware with Probe in Place.

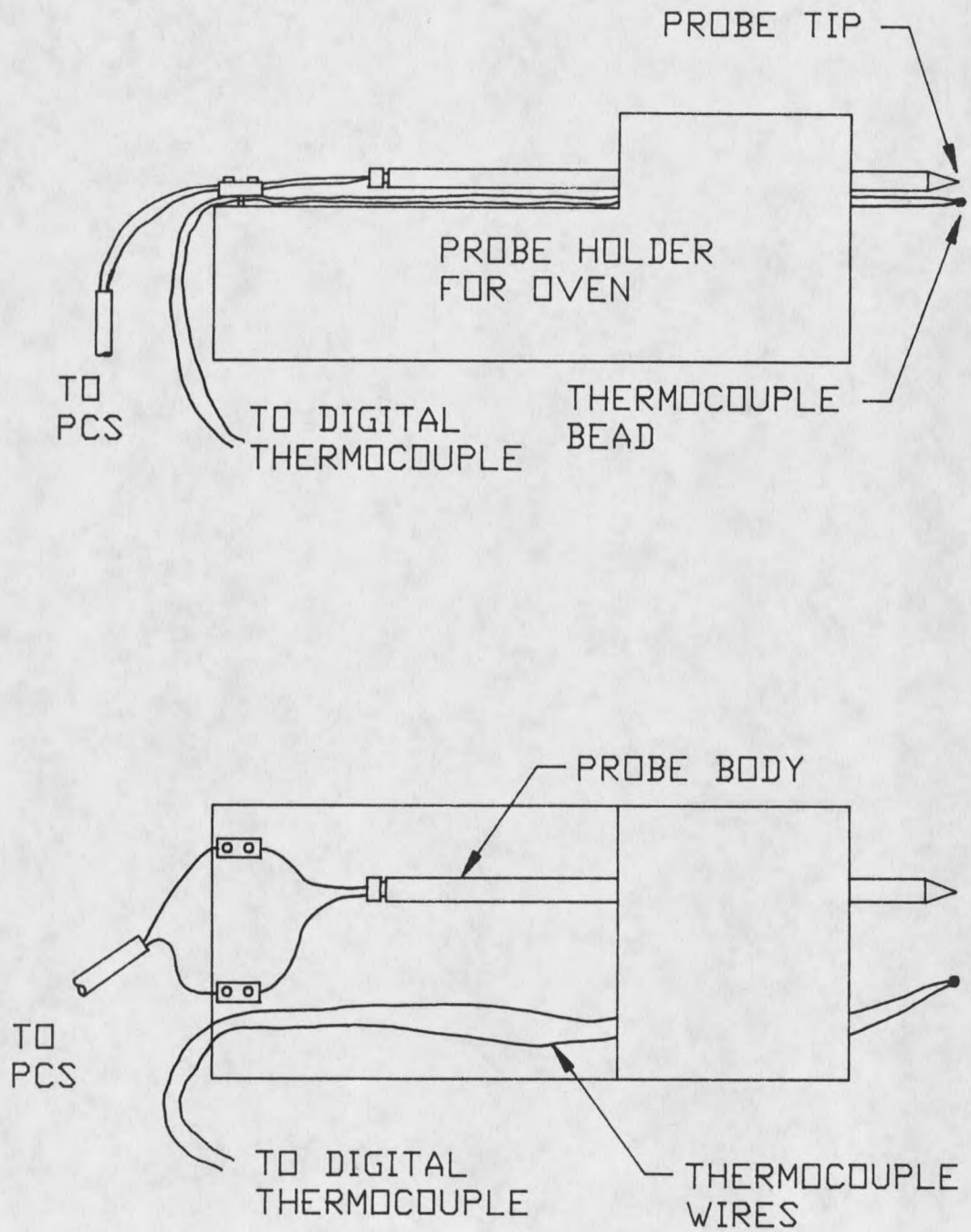

Figure 11. Probe and Accompanying Thermocouple in Probe Holder.

Low Velocity Tunnel (LVT)

The low velocity tunnel (LVT), shown in Figure 12, is a fan-operated venturi manufactured by Aerolab Supply Company. Air flows through the tunnel by suction induced by the fan at the exit of the tunnel. The amount of mass passing through the test section is controlled by letting air enter behind the test section through the gap in a cylindrical shroud enclosing the test section, thereby decreasing the mass flow entering ahead of the test section. By controlling the gap width one can change the velocity in the test section and thereby obtain a Reynolds number range of about 1700–9000 per cm.

The probes were mounted on a holder, shown in Figure 13. The holder positioned the probe on the centerline of the LVT directly facing into the flow.

The LVT was calibrated with a pitot-static tube and a vertical manometer using water as the working fluid. Incompressible flow was assumed in calculating the velocity yielding the following formula for velocity:

$$V = \left[2gy\left(\frac{\gamma_{H_2O}}{\gamma_{AIR}} - 1\right)\right]^{1/2} \quad \text{(m/s)} \quad . \tag{54}$$

The calibration measurements were made at the tunnel centerline, where probes would be positioned, with the probe holder stand in place. Results were cross checked by using a separate manometer, static, and dynamic pressure taps. The range of velocities for the LVT were found to be from about 2.6 m/s to 16.0 m/s at the maximum with an error of about 0.1 m/s. The calibration of test section velocity versus gap width is shown in Figure 14.

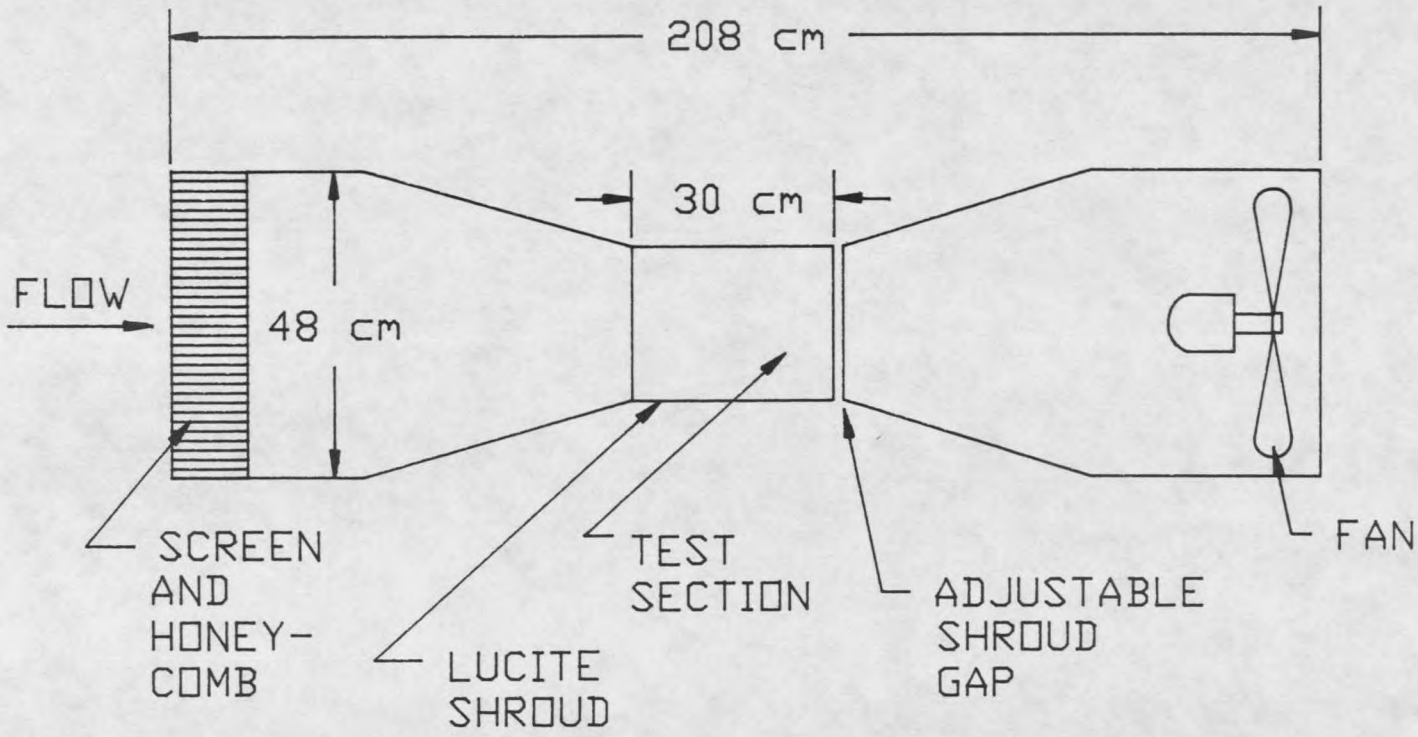

Figure 12. Low Velocity Tunnel.

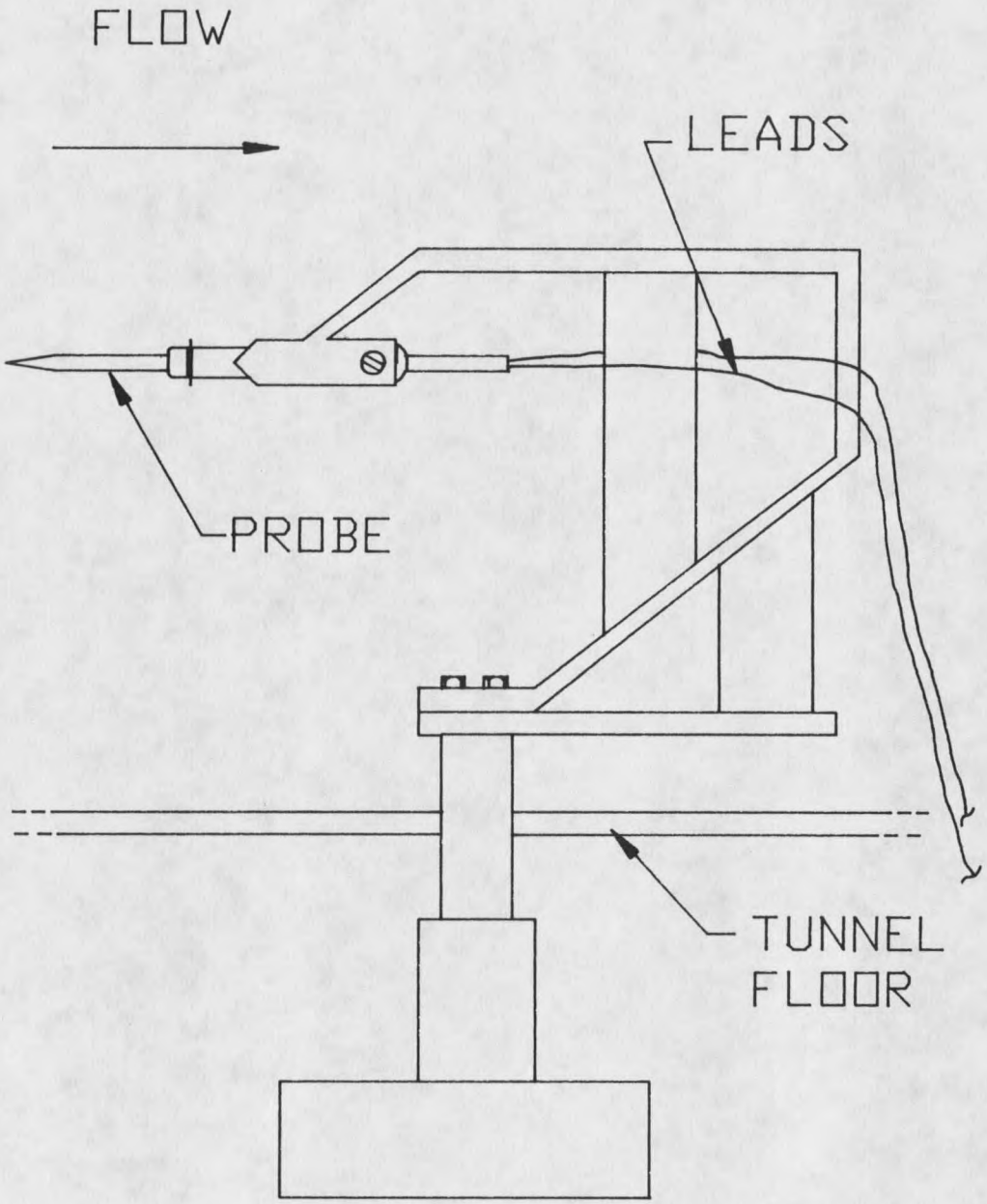

Figure 13. Probe Holder for Low Velocity Tunnel.

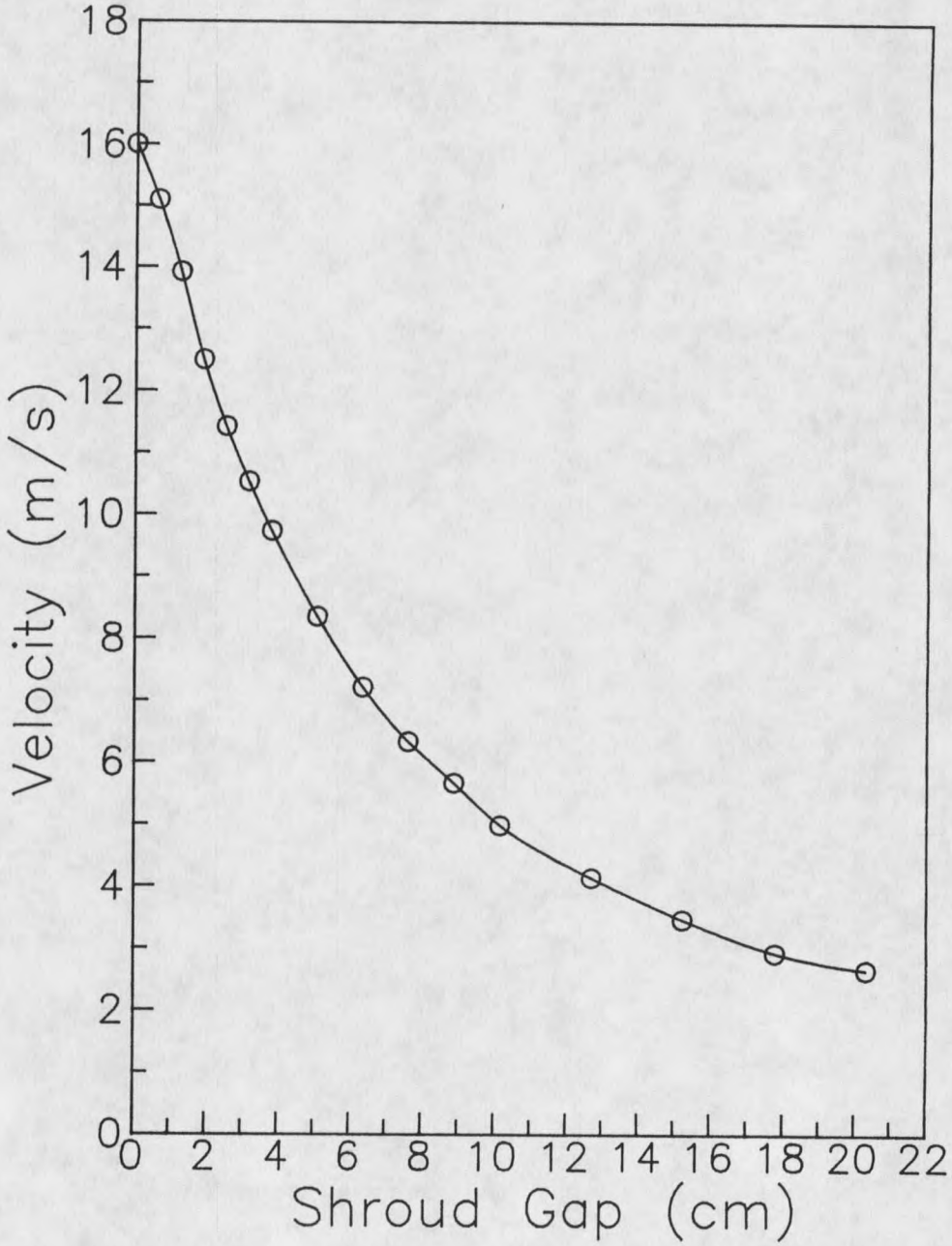

Figure 14. Calibration Results of Low Velocity Tunnel.

Supersonic Wind Tunnel (SWT)

The Montana State University Supersonic Wind Tunnel is of an open circuit type, using air as the working fluid. The flow is continuous for a period of several hours, being limited by the ability of the silica-gel air dryer to maintain a dew point of about -34 C. The present setup allows for Mach numbers as high as 3 and Reynolds numbers from about 19,000 per centimeter to about 120,000 per centimeter. These flows are obtained by a two-dimensional Mach 3 nozzle block. Also, stagnation temperatures can be obtained between about 10 C to 65 C. The geometry of the test section itself is about 7.9 cm $\times$ 8.1 cm $\times$ 40.6 cm.

The general circuit and its components are shown in Figure 15. Atmospheric air first enters and passes through a silica-gel air dryer in order to remove as much moisture as possible. It then passes through a throttling valve, which controls the stagnation pressure, and then goes into a stilling tank before entering the test section. The air then passes through the supersonic nozzle, through the test section, and into the supersonic diffuser. From there, it flows through a subsonic diffuser, two pumping stages and a large silencer after which it is exhausted to the atmosphere.

The Supersonic Wind Tunnel is controlled from a console located near the test section. The console allows the operator to adjust the temperature and the inlet pressure. These settings can be controlled automatically or manually. For more information on the SWT see [23].

The hot-film probes were mounted on the center line of the SWT. The local Mach number was changed by moving the hot-film probe to different positions along the tunnel axis. The Mach numbers greater then one were found by using a transducer calibrated to obtain the pitot pressure as in Figure 16, the SWT control

gauge to obtain the stagnation pressure, and the isentropic charts to determine the Mach number at that corresponding pressure ratio. The pitot probe was arranged to be at the same axial position as the probe at about 1.25 cm to one side. Figure 17 shows the film probe holder with accompanying pitot probe. The pitot probe also allowed the operator to determine if the flow near the probe tip was unsteady or not. The position at Mach 1 was simply at the throat and for Mach numbers less than one the position was determined by using Figure 18.

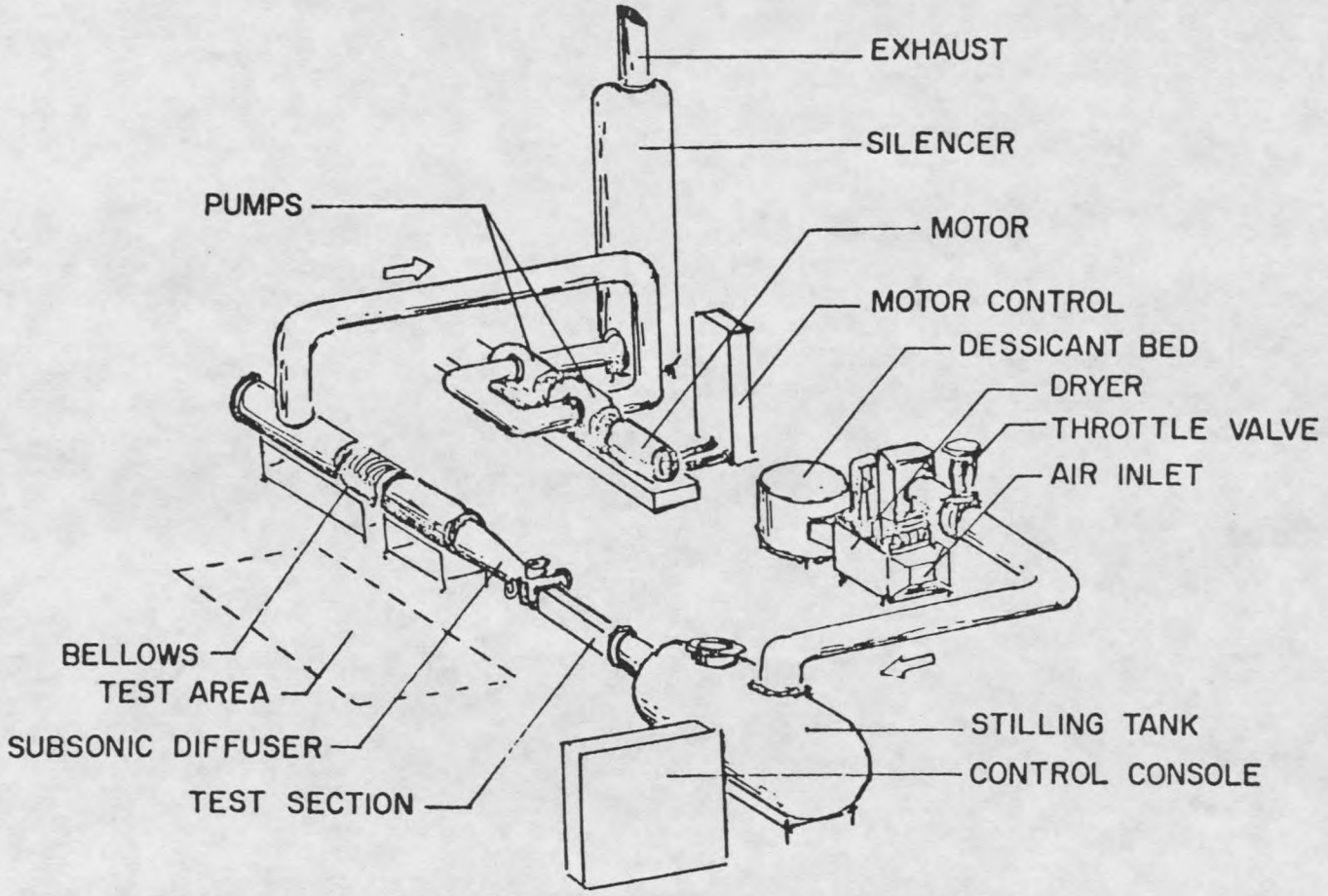

Figure 15. General Circuit of Supersonic Wind Tunnel.

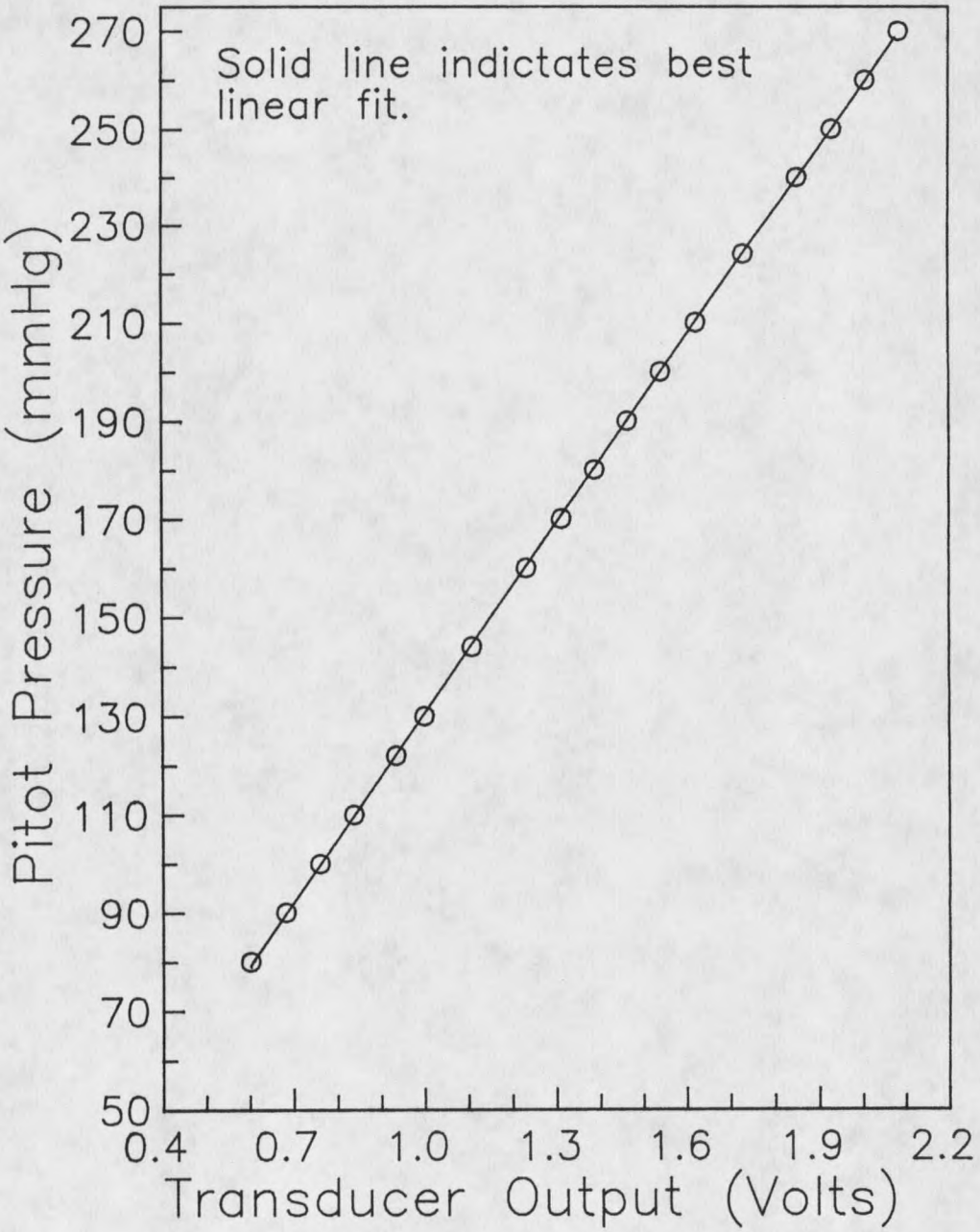

Figure 16. Transducer Calibration for Measurement of Pitot Pressure in Supersonic Wind Tunnel.

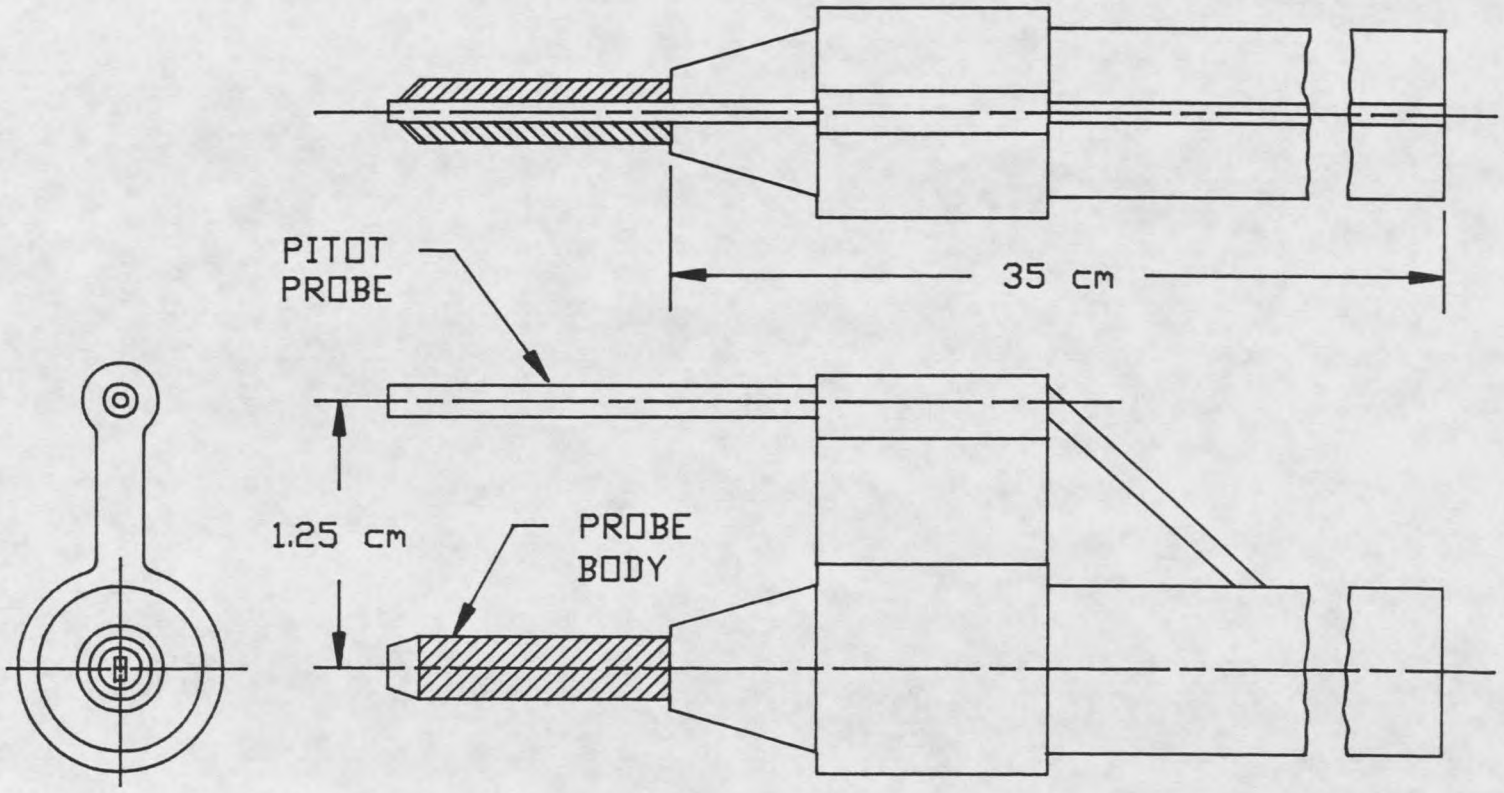

Figure 17. Supersonic Wind Tunnel Film Probe Holder with Accompanying Pitot Probe.

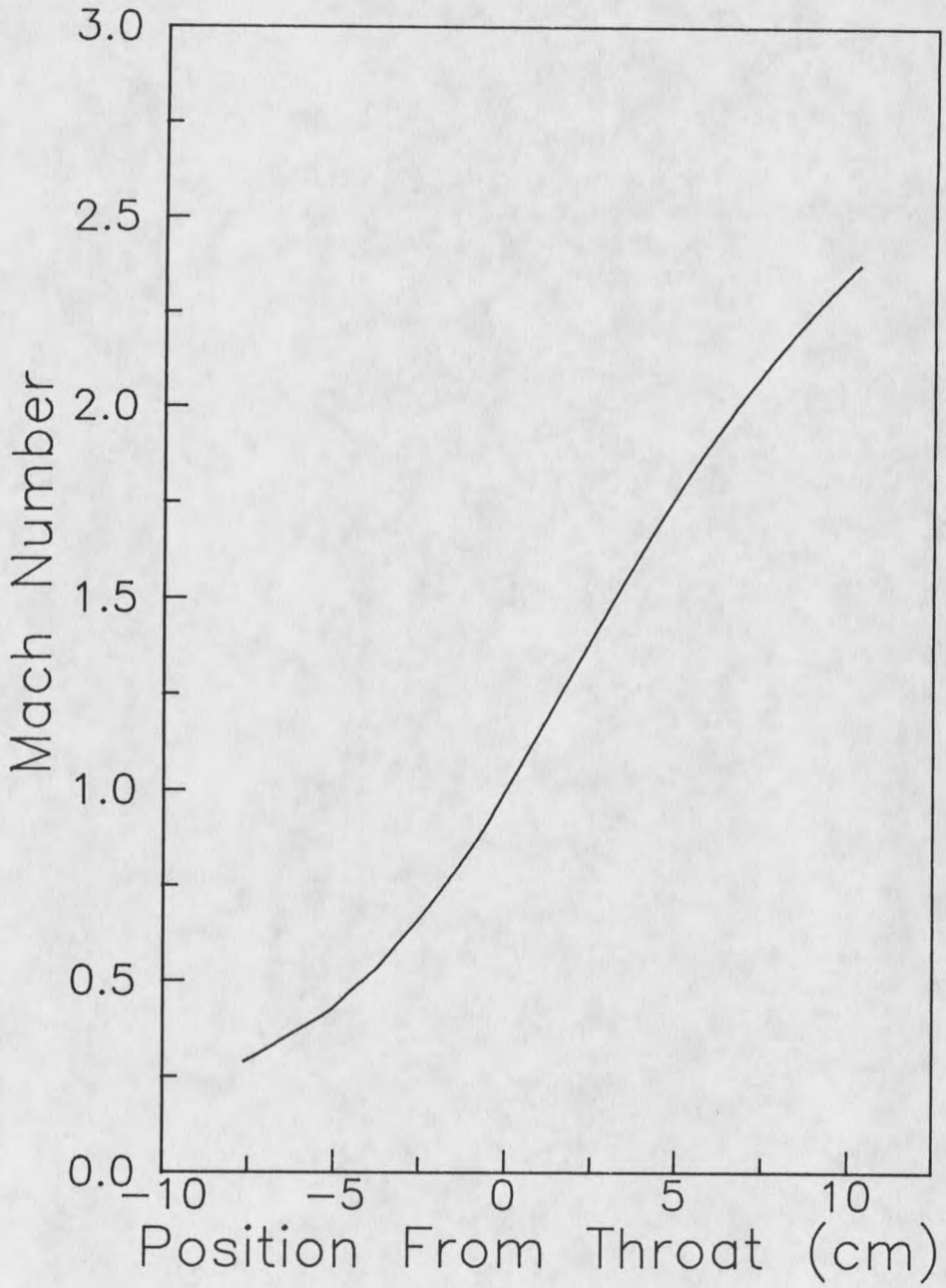

Figure 18. Mach Number Variation With Position.

CHAPTER 7

CALIBRATION PROCEDURES

Oven Calibration Procedures

In order to determine the resistance-temperature relation of each probe it is necessary to perform an oven calibration. This calibration is performed using the PCS and oven calibration hardware described in Chapter 6. The desired results of this calibration are the reference resistance at 0 C and the resistivity coefficients α and β. These variables are used to find the probe temperature at zero current and to find the measured Nusselt number. In order for the probe to be of any use these variables must be known accurately. The following is an outline of the procedure. For detailed step-by-step instructions see Demetriades [7].

After mounting the probe and thermocouple in the oven probe holder as previously shown in Figure 10 the oven is activated. The oven is then allowed to reach a temperature of 500 C which takes about one hour. At this point the cable linking the probe lead wires to the PCS is connected. The PCS is then programmed to take an overheat traverse of specified magnitude and length at several temperatures (20 currents, 100 mA maximum current, and 17 different temperatures at 30 C steps, for instance). Upon finishing the programming, the oven power source was shut off so that the oven would begin cooling. The calibration is then started by the operator so that the first overheat traverse is taken at 500 C. After this data set is taken the operator names the file to be written to. The PCS can now be left to finish the calibration automatically. After about a 12 hour period the

calibration is complete with the data stored in the specified file. The probe is then withdrawn from the oven and the PCS deactivated.

The program to be used with the PCS is named WIRECAL. Having the data from the oven calibration on disk, the data are then reduced using a program named NEWOVEN.BAS (see Appendix C). This program can produce either a detailed or a summarized view of the oven calibration results. A typical summarized view is the one-page output of Figure 19. As shown in this figure, the output gives a table of oven temperature versus hot-film resistance and these important results: probe resistance at zero current and zero degrees C, the first resistivity coefficient (α), and the second resistivity coefficient (β). The program also prepares a summary file that is used to produce graphical results of temperature versus resistance as will be presented in Chapter 8. In order to produce this graph the overheat traverse at each oven temperature was fit with a second degree polynomial to find the resistance at zero current for that temperature. This results in a set of data containing zero current resistances versus the corresponding temperatures. These data are also fit with a second degree polynomial to find the reference resistance and the coefficients of resistivity.

The calibration is done in order to find how the resistance of the film increases with temperature. Unless compensation is made, the actual relation found includes the resistance of the film, its corresponding platinum lead wire, and possibly its connecting cable increases with temperature. This is true for both oven and flow calibrations. For probes operating over wide temperature ranges this may become very important as it may otherwise give erroneous results of the probe measurements. In order to avoid this, the values of the resistance of the cable and lead wires at their corresponding temperatures are subtracted from the measured resistance so that the resulting value is the film resistance alone.

NEWOVEN DATA REDUCTION PROGRAM

DATE 3-07-90
PROBE NUMBER 50
CALIBRATION FILE NAME a:5030790.ov9

CABLE RESISTANCE RECORDED .166
LINE RESISTANCE (OHMS) = .166 + .1381497 * (1 + .003927 * T)

THE MAXIMUM SET CURRENT WAS 100 mA
THE MAXIMUM CURRENT ACHIEVED WAS 97.715 mA
THE NUMBER OF CURRENTS USED WAS 20

TEMP DEG. C	R OHMS	D	CRIT. C mA
498	15.28	-.219	289.22
466	14.87	-.128	292.12
436	14.38	-.271	284.91
406	13.88	-.334	276.87
377	13.4	-.197	277.9
347	12.93	-.042	277.42
317	12.38	-.174	267.09
287	11.85	-.098	265.46
257	11.31	.123	266.63
229	10.86	-.069	259.17
199	10.35	.103	260.25
169	9.82	-.138	252.43
139	9.28	.133	254.19
109	8.74	.104	249.28
79	8.18	-.104	242.04
50	7.62	.015	239.88
27	7.17	-.207	230

THE MAXIMUM RESISTANCE FOR THIS PROBE (OHMS)= 17.17468
THE LARGEST PERCENT OVERHEAT ACHIEVED = 20.91941
THE LARGEST POWER DISSIPATION (mW) = 163.9876
MAXIMUM PROBE TEMPERATURE ACHIEVED = 596.5743

RO (OHMS, AT 0 DEG. C)= 6.842243
ARO (OHMS/DEG C)= 1.731961E-02
AVERAGE RESISTANCE-CURRENT DEVIATION. (OHMS)= 3.010654E-03
OVERALL RMS DEVIATION OF R FROM R-T CURVE (OHMS)= 1.716214E-02
THE AVERAGE VALUE OF THE CONSTANT D = -8.790911E-02
ALPHA (REFERRED TO RO ABOVE,PER DEG. C)= 2.531277E-03

QUADRATIC FIT OF RESISTANCE -VS- TEMP.
RESISTANCE AT ZERO DEG. = 6.678555
QUADRATIC ALPHA = 2.867842E-03
QUADRATIC BETA = -5.285644E-07

Figure 19. Summarized Output for Oven Calibration for Probe Number 50.

This total line resistance is given as

$$R_T = R_{LW} + R_C \quad . \tag{55}$$

Using the known resistance and resistivity of 24-gauge platinum wire the platinum lead wire resistance is approximately

$$R_{LW} = 0.138(1 + 0.003927 * T) \quad . \tag{56}$$

The cable resistance can be measured directly. For the oven calibrations the cable remains at room temperature the entire time so that no temperature compensation is needed. If the cable was subject to heating an equation similar to that for the platinum lead wires could be written.

Flow Calibration Procedures

The flow calibration procedures are explained in [7] as they are written here. The procedure for flow calibration in the LVT consists of first mounting the probe along the center-line of the LVT and then connecting it to the PCS. One overheat traverse is performed at zero velocity. The LVT is then started and a shroud gap is chosen. An overheat traverse is performed, the data is stored, and the velocity is noted. The velocity of the LVT is then changed and another overheat traverse is performed. This cycle continues until approximately fifteen overheats have been performed at known velocities. The flow properties are determined using atmospheric pressure and the temperature measured at the LVT inlet. The data is then reduced using the program FLOWRDCT.BAS (see Appendix D).

The procedure for flow calibration for the SWT is similar to the procedure for the LVT except that for the LVT only the velocity is changed for each overheat traverse while for the SWT the temperature, pressure, and Mach number are

varied for each traverse. The SWT flow calibration procedure begins with first mounting the probe in the SWT and then starting the tunnel and bringing it to the appropriate temperature. The probe is then moved to the position of the desired Mach number at the tunnel center-line. The connection to the PCS is made at this time. Having recorded the Mach number, total temperature, and stagnation pressure an overheat traverse is made. This file is then saved for later reduction. The stagnation pressure of the SWT is then changed by about 20 mm Hg and another overheat traverse is made. This cycle of recording the flow parameters and making overheat traverses continues until the lowest pressure obtainable without flow "break-down" is reached. After reaching the lowest pressure, the pressure is returned to its maximum and another Mach number is selected. The cycle begins again and continues for each Mach number. After taking data for each desired Mach number the tunnel stagnation temperature is changed and the entire routine is repeated. The calibration routine used included Mach numbers 3, 2, 1, and 0.5 and stagnation temperatures of about 15 C and 65 C. The pressure ranges were from about 615 mm Hg to 100 mm Hg at a minimum. The resulting unit Reynolds number range was from 25,000 to 120,000 per centimeter.

This process results in about 4000 points of data. The program FLOWRDCT.BAS (Appendix D) was written and used to reduce this data.

CHAPTER 8

RESULTS

Temperature Endurance and Stability

For the film anemometer probes to be of any use in high temperature hypersonic flows it had to be determined through experimental testing if they could withstand the high temperatures and remain stable.

In order to test the temperature endurance of the film anemometer probes they were placed in a high temperature environment. The maximum temperature was typically around 700 C. The resistance was then monitored for a period of over two hours. A constant resistance over time for several high temperatures indicated that the film was stable under these conditions. It was found that probes that failed to maintain a constant resistance were most likely to be the probes that failed in future tests. The stability could also be monitored by noting the difference between the resistance before and after the soak. Typical changes were 0.2 ohms.

In order to further test the stability and endurance of the film anemometer probes, several destructive tests were performed. Four probes were used to determine the highest survivable operating temperature of the probe and to see if probes could remain stable over time. Note that "operating temperature" refers to the film temperature upon applying the heating current and not to the temperature of the medium surrounding the film alone. These tests revealed several significant findings. One finding was that probes could be pushed to at least a

90% overheat (percent increase in resistance). This overheat resulted in a film temperature of 356 C above room temperature. Limitation on the maximum current of the programmable current supply restricted any higher overheats. Other tests which were performed were aimed at finding the maximum operating temperature of the hot-film probe. Previous to these test the maximum film operating temperature obtained in a successful oven calibration was 665 C. High operating temperatures can be achieved by either raising the temperature of the medium and keeping the overheat approximately constant (about 25%) or by raising the overheat at a constant but relatively high surrounding temperature (500 C in this case). The highest film temperature achieved by the fist method (raising the oven temperature) was 765 C. The probe characteristics shifted slightly at this temperature indicating that the temperature limit had been exceeded. The next highest film temperature achieved by this method without a resistance shift was 725 C. This indicated that the maximum operating temperature for this probe was about 750 C. The second method of reaching high operating temperatures (by increasing the overheat) found the highest film temperature achievable to be 800 C. The film's resistance shifted at this temperature and then failed, indicating that the maximum operating temperature had obviously been exceeded. However, before failing, the film anemometer indicated a temperature of 765 C without any apparent shifting of the film's resistance. This was considered the maximum operating temperature of this film anemometer as it previously existed. Though the two methods for reaching high operating temperatures differed, the results of both tests agree fairly closely. It appears that the maximum operating temperatures of the particular probes studied here are around 760 C. High temperature survivability is very important for the application being sought but is not the only criterion the probes must meet. The probes must also be stable.

Stability of the films was examined by constant room checks and repeated oven calibrations. Probes demonstrated a tendency to drift to a higher resistance as they aged and underwent repeated calibrations (about 0.2 ohms or 2% was typical). Probes that were unstable (changed more that 2 ohms) typically failed in later testing.

Probes incapable of surviving high temperatures or remaining stable were eventually destroyed and rebuilt. If they could not successfully endure these tests they were determined to be of no use since the rest of the film's history would rely on them.

Dynamic Pressure Endurance

If probes were to be used in hypersonic flows they must be able to endure high dynamic pressure loads inherent in these types of environments. A select few of the probes used were placed in a Mach 6 high dynamic pressure facility in order to find out if the films could survive. The probes were found to survive dynamic pressure loads of 160 kPa (23 psia) before failing (hot-wires are typically limited to dynamic loads of about 30 kPa (4 psia)). Though the films did finally fail at these loads it is believed that failure occurred due to particle impact combined with high dynamic pressure and not due to high dynamic pressure alone. This would make sense physically since the film has a hard backing, unlike the hot-wire probe, and should therefore be able to withstand very high "clean" dynamic pressure flows. Microscopic inspection of the films indicated that particle impact had caused the failure.

Resistance and Resistivity Coefficients

The reference resistance and the coefficients of resistivity were obtained as outlined in Chapter 7. Since every probe had different physical characteristics, each had to be oven calibrated. It is not sufficient to determine the reference resistance alone and then apply the tabulated values for the resistivity coefficients of platinum. Resistivity coefficients are often quoted for the bulk material and are likely to be different (Lomas [3]) for very thin samples (films were about .0000013 cm thick according to Demetriades [9]). Also, the platinum film resinate could easily contain impurities that would be reflected in the value of the resistivity coefficients. For these reasons each film is oven calibrated. Table 1 shows results of 39 oven calibrations. The average α value is .00293 $\frac{1}{C}$ and the average β value is -.00000071 $\frac{1}{C^2}$ with standard deviations of .00014 $\frac{1}{C}$ and .00000020 $\frac{1}{C^2}$, respectively. These standard deviations of 5% and 28% speak of the predictability of the resistivity coefficients for these sensors. These values are reasonably close to those quoted by Perry [1] and Hinze [14] of .0035 $\frac{1}{C}$ for α and -.00000055 $\frac{1}{C^2}$ for β for platinum. Note that for the film anemometer probes studied the oven calibration is fit with a second degree polynomial to find α and β. Typical oven calibration results are presented on a summary page as in Figure 19 and in graphical form as in Figure 20. Hot-wires were typically fit with a best linear fit ($\beta = 0$). For the targeted temperature range a linear fit was found insufficient for the films, as will be demonstrated.

The effect of the proper type of fit of the oven calibration data was found to be very significant for the film anemometers studied. Figures 21 through 23 show this effect. Originally a linear fit was thought sufficient and flow calibration data were reduced as shown in Figures 21 and 23.

OVEN CALIBRATION RESULTS SUMMARY

PROBE TEST	R_r	$\alpha \times 10^3$	$\beta \times 10^7$
59OV1	6.614	3.053	-10.36
59OV2	6.745	2.961	-9.898
58OV1	8.090	2.824	-6.712
58AOV1	10.087	2.946	-9.544
57OV1	11.465	3.190	-7.151
57OV2	12.164	3.214	-7.379
56OV1	14.362	2.973	-7.084
56OV2	15.358	2.837	-6.532
55OV1	14.151	2.866	-10.94
55OV2	14.487	2.749	-7.458
54OV1	22.315	2.648	-6.522
53SOV1	13.471	2.697	-8.046
53OV1	6.587	3.007	-8.276
53OV2	6.637	3.021	-8.149
52OV1	8.765	3.202	-12.17
52OV2	9.322	3.031	-12.52
51OV1	12.407	2.870	-6.428
51AOV1	7.902	3.278	-8.614
50OV1	6.852	2.985	-6.439
50OV2	6.836	2.939	-5.984
50OV3	6.845	2.864	-4.867
50OV4	6.757	2.912	-5.236
50OV5	6.746	2.952	-6.004
50OV6	6.526	2.821	-3.265
50OV7	6.416	3.038	-6.990
50OV8	6.400	3.074	-7.655
50OV9	6.679	2.868	-5.285
49OV1	15.611	3.026	-6.393
49OV2	16.955	2.927	-6.469
49OV3	17.086	2.905	-6.071
49AOV1	8.843	2.876	-5.306
48OV1	7.177	3.007	-6.287
47OV1	14.862	2.791	-5.403
46OV1	9.315	2.850	-6.215
45OV1	12.252	2.753	-4.841
44OV1	13.073	2.833	-6.324
43OV1	15.250	2.799	-5.077
43AOV1	12.305	2.813	-6.227
42AOV1	26.009	2.734	-5.840
AVERAGE		2.926	-7.076
STANDARD DEVIATION		0.144	2.005

Table 1. Resistivity Coefficients for 39 Oven Calibrations.

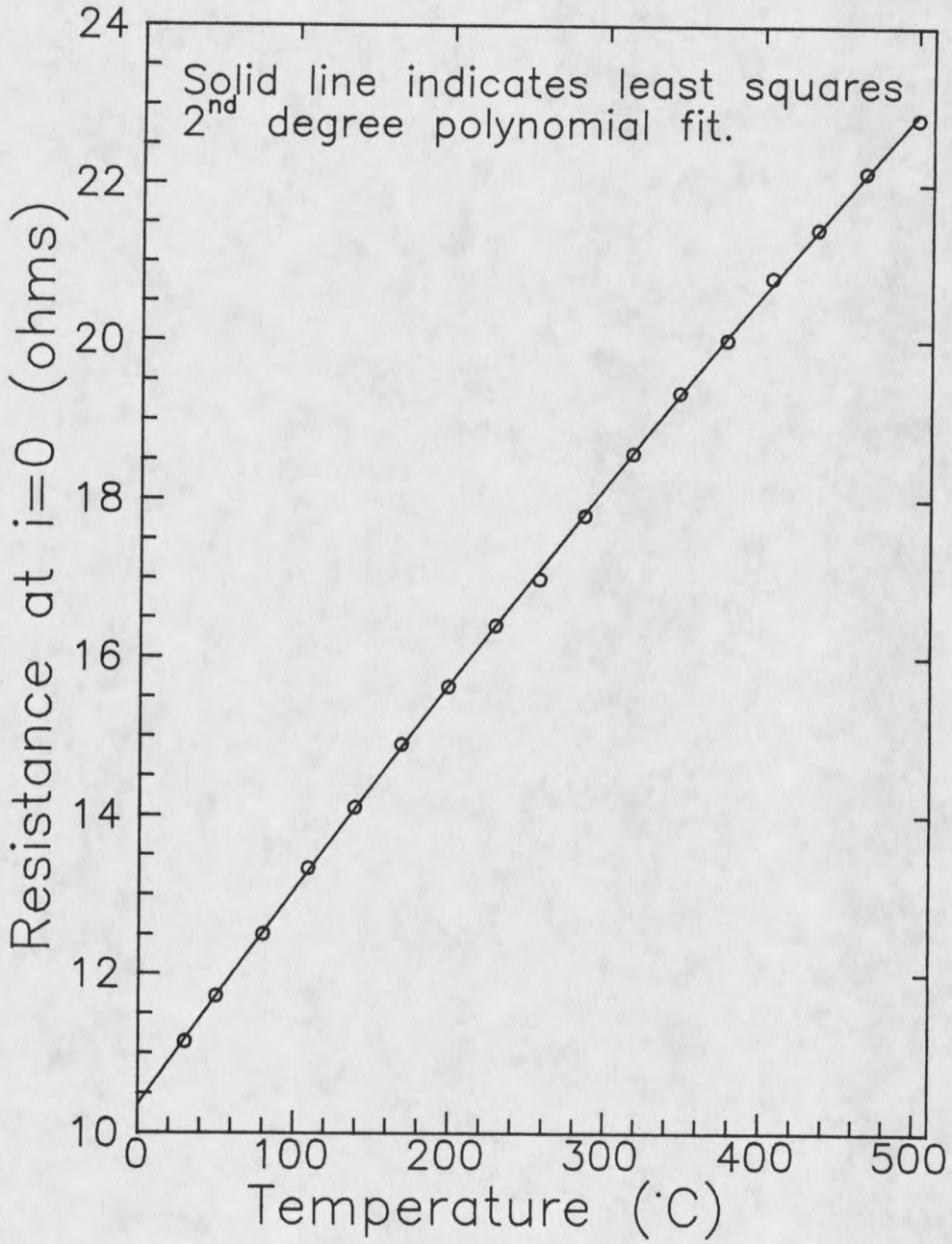

Figure 20. Graphical Presentation of Oven Calibration Results for Probe 48.

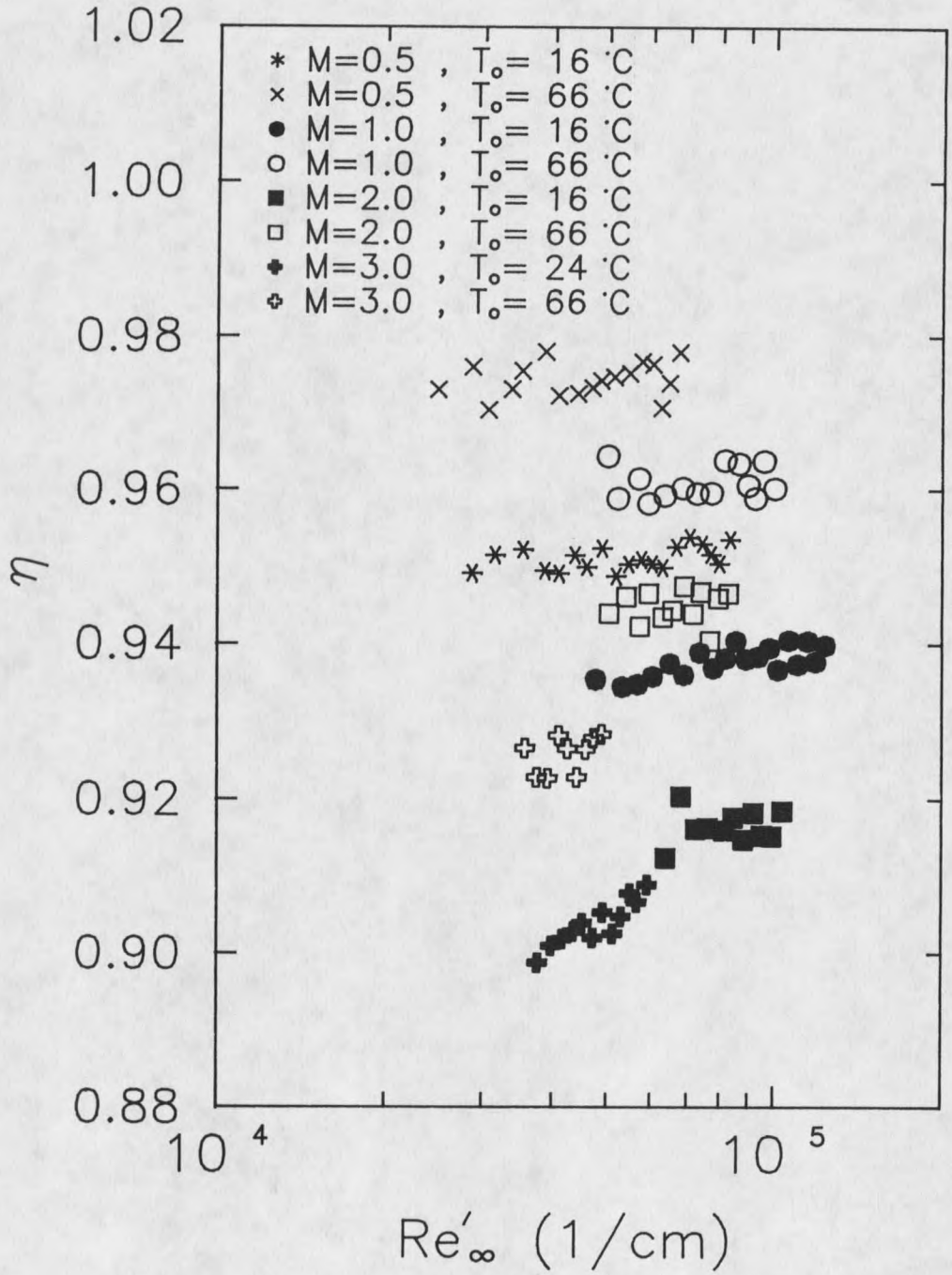

Figure 21. Temperature Recovery Factor Variation for a Typical Probe. Resistivity Calibration with $\beta = 0$. Resistance versus Power Data Fit with a Second Degree Polynomial.

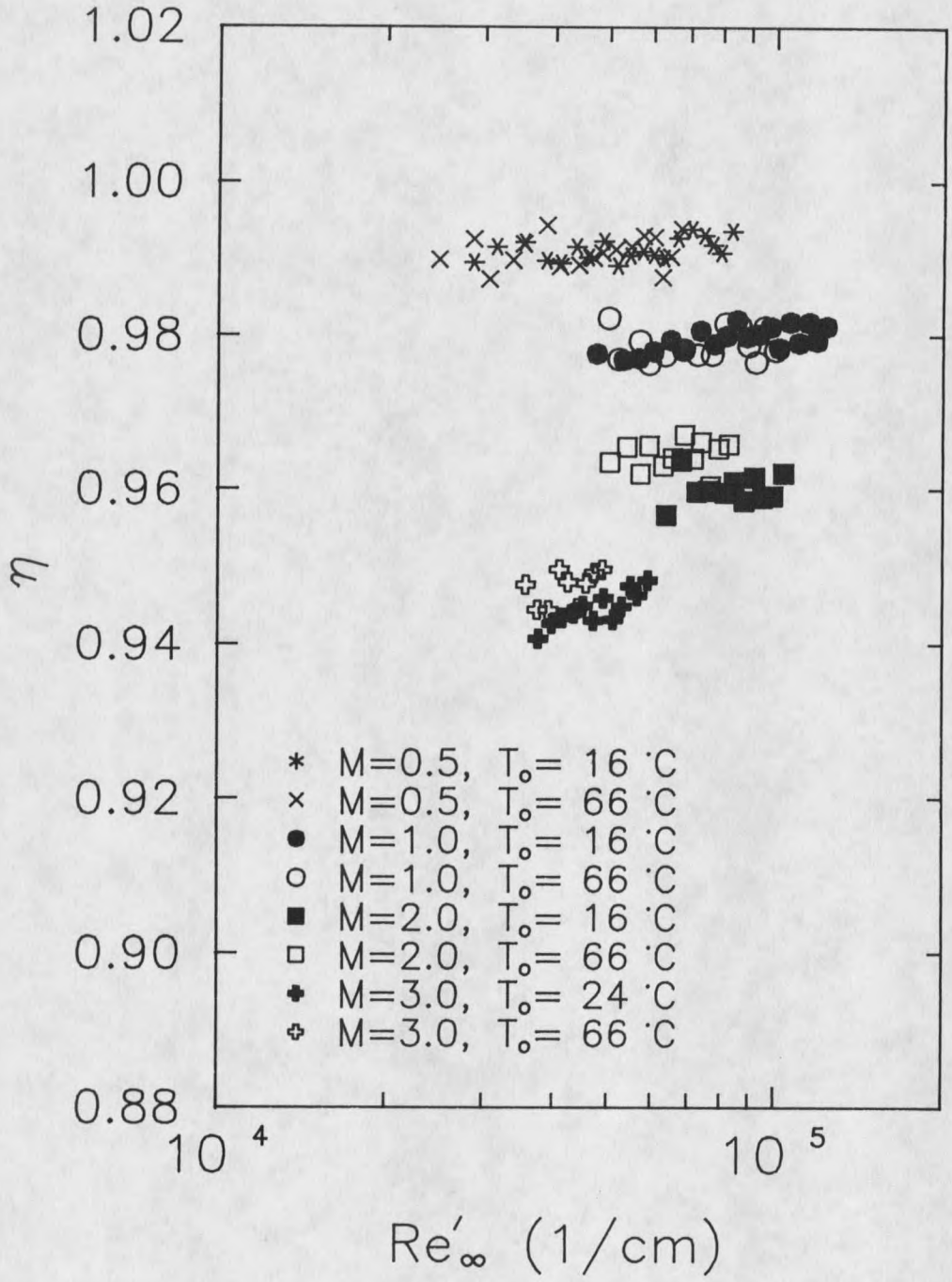

Figure 22. Temperature Recovery Factor Variation for a Typical Probe. Resistivity Calibration with $\beta \neq 0$. Resistance versus Power Data Fit with a Second Degree Polynomial.

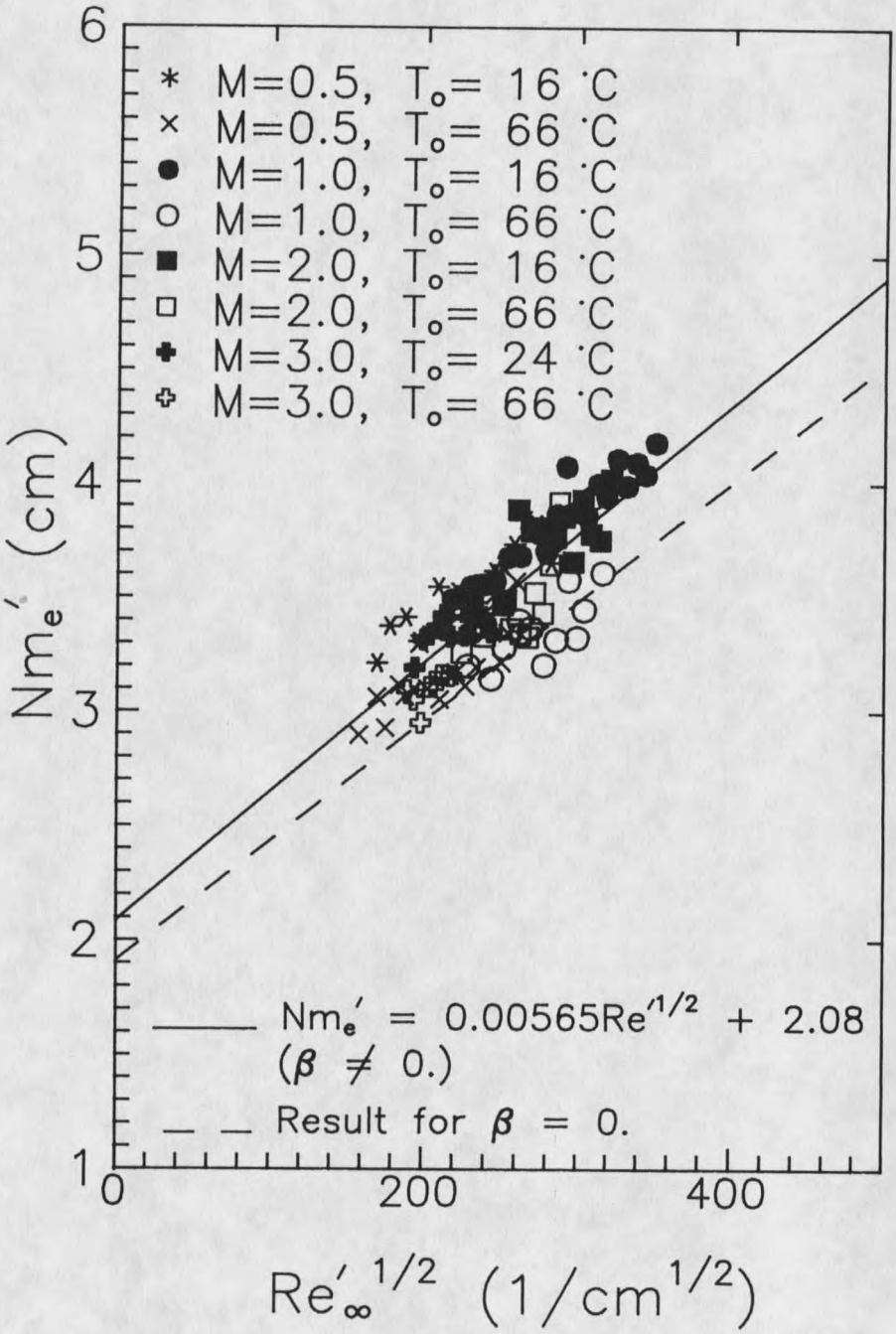

Figure 23. Heat Transfer Characteristics for a Typical Probe. Resistance versus Power Data Fit with a Second Degree Polynomial.

The temperature recovery factor is shown to be a function of both stagnation temperature and Mach number. Upon using a second degree fit of the oven calibration data instead of a linear fit the same flow calibration data were found as shown in Figure 22 and 23. Figure 23 shows a definite shift in the Nusselt number results. The dotted line represents the best linear fit of the data reduced using the linear oven calibration results ($\beta = 0$). Figure 22 shows that the temperature recovery factor is not a function of stagnation temperature as compared with the same data in Figure 21 reduced with a linear oven calibration. The data presented in Figure 22 indicated that the temperature recovery factor is a function of Mach number and slightly of Reynolds number for Mach 3.

Dependence of The Nusselt Number On Power

In Chapter 5 it was noted that the Nusselt number was dependent on power. A constant D was then defined that would give indication of how the Nusselt number depends on power. This constant D was plotted against the flow Reynolds number in order to investigate this power dependence. The list of variables in Figure 19 also includes the constant D. This list gives typical results of how the probes behaved and shows that the absolute value of the constant D generally increases as the surrounding medium increases with temperature. Figures 24, 25 and 26 show how the constant D is related to Mach number, Reynolds number, and stagnation temperature. The value of D generally remains unaffected by all variables except the stagnation temperature for the entire range investigated.

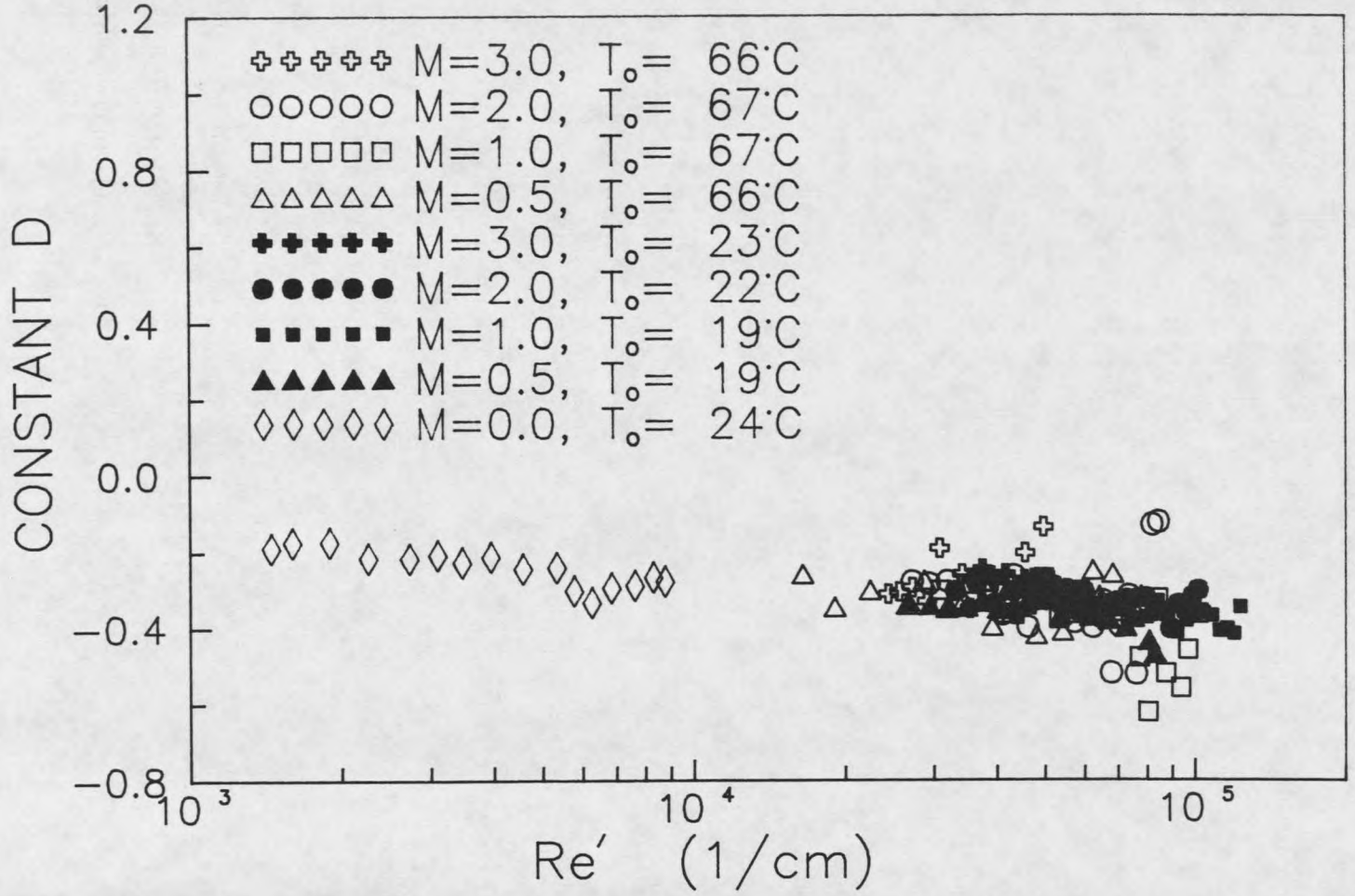

Figure 24. Characteristics of the Constant D for Probe 48.

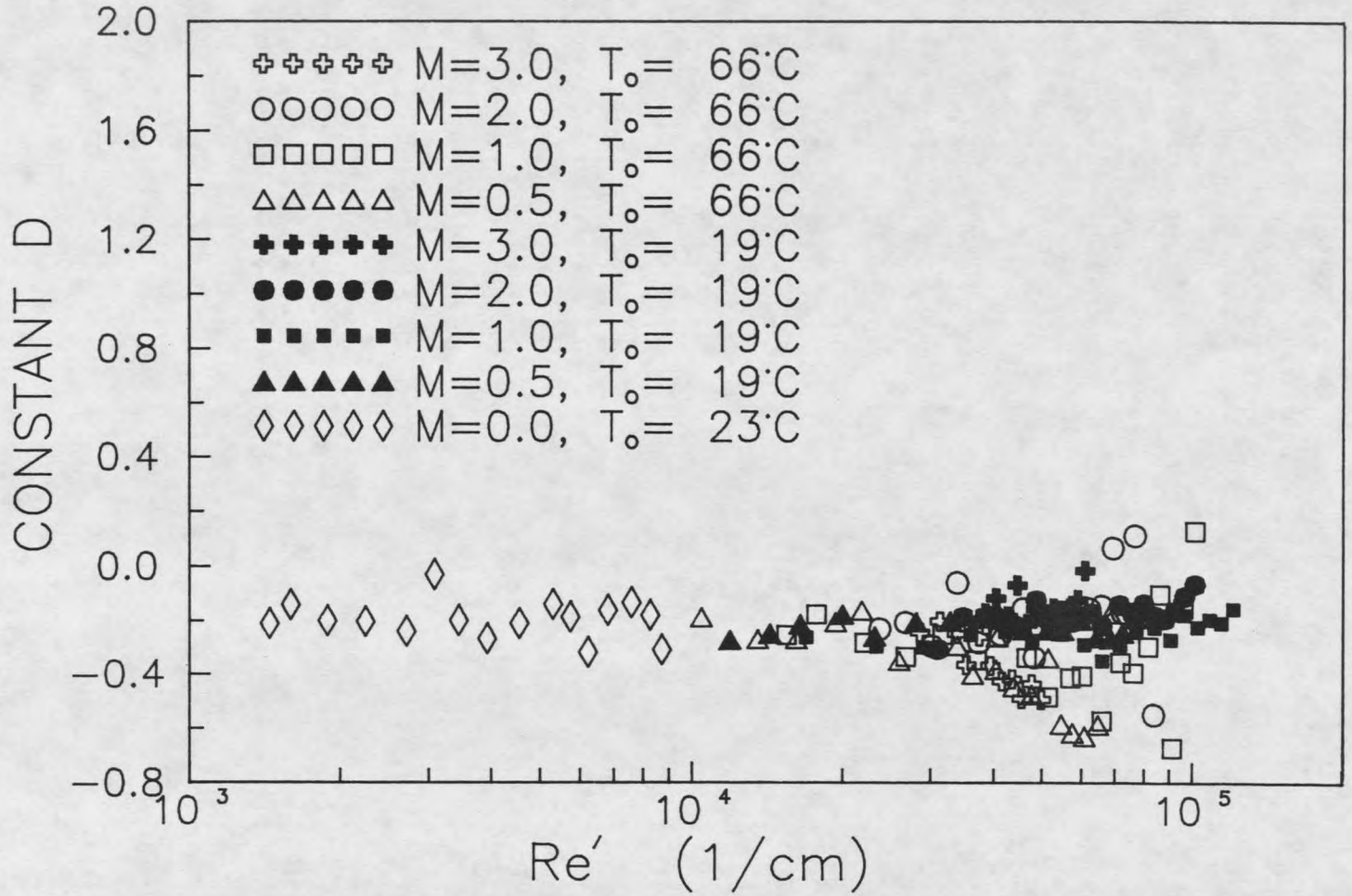

Figure 25. Characteristics of the Constant D for Probe 50.

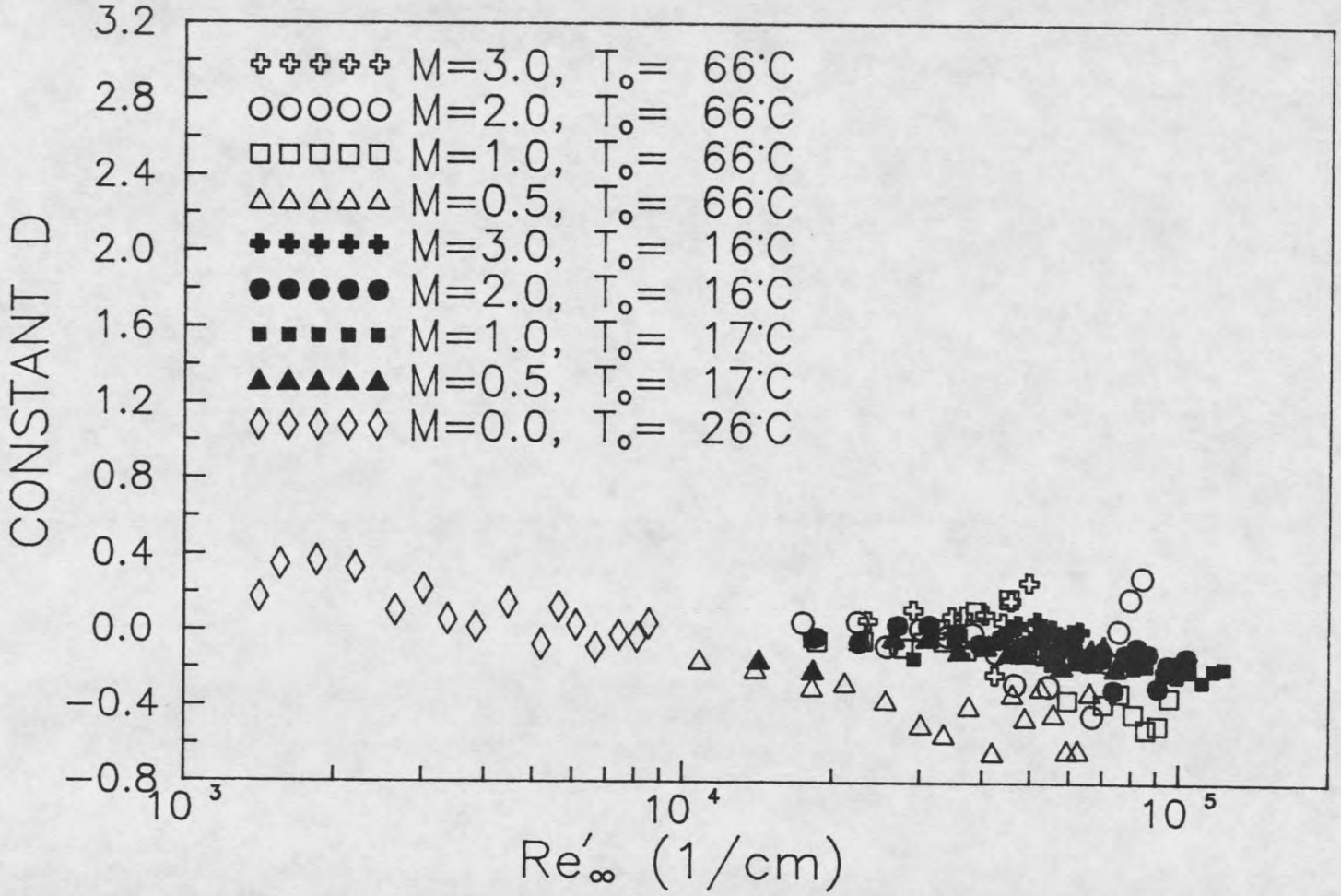

Figure 26. Characteristics of the Constant D for Probe 56.

Temperature Recovery Factor Dependence on Flow Properties

If calibrated correctly the film anemometer probes could be used to determine certain flow properties such as the stagnation temperature and the unit Reynolds number as well as the relations necessary to make turbulence measurements. The correct calibrations are those which give these necessary heat transfer characteristics of the film anemometer. By knowing and understanding these, the calibration data can be used most effectively.

Through constant experimental work over a period expanding approximately three years both oven and flow calibration data have been taken and reduced in order to determine the hot-film probe characteristics. The two most telling parameters found from a flow calibration are the temperature recovery factor and the Nusselt number. Together they can be used to find information about the flow. The temperature recovery factor can ideally be related to the stagnation temperature of the flow knowing the Mach number or to the Mach number knowing the stagnation temperature. The Nusselt number can be related to the free-stream Reynolds number. Obtaining these relations is also the first step necessary in order to make turbulence measurements.

The temperature recovery factor is found by relating the film resistance at zero current to the recovery temperature of the flow by an oven calibration and then dividing this result by the stagnation temperature of the flow. Its value depends on the local free-stream Mach number and the frictional dissipation of the kinetic energy in the boundary layer (Kovasznay [11]). For the film anemometers studied here the temperature recovery factor was typically close to 1.02 at a Mach number of 0. This indicates that the probe is not a very good instrument for measuring the temperature of the surrounding medium. A temperature recovery

factor of 1.02 indicates that the probe will measure a temperature 2% higher than the actual absolute temperature. This would result in an error of 6 C for a measurement taken at room temperature. This poor temperature measurement capability is most likely caused by shifts in the probe resistance. Even small shifts (about 0.2 ohms) will cause poor results such as the ones found. From a value of about 1.02 for a Mach number of 0 the temperature recovery factor decreased with increasing Mach number to about 0.8 at Mach 8. Figures 27, 28 and 29 show typical results of how the temperature recovery factor varied with the various flow parameters for Mach numbers of 0, 0.5, 1, 2 and 3. Figures 30 and 31 show results of a Mach 8 calibration. Figure 32 is a plot of Mach number versus the normalized temperature recovery factor. The temperature recovery factor was normalized by dividing the results for each probe by its value at Mach 0. This was done so that different probes could be compared on the same plot. The figure shows clearly that the temperature recovery factor decreases with increasing Mach number. It is expected that this Mach number dependence will disappear as the Mach number approaches infinity. The data appear to draw this conclusion. This data of Figure 32 should be looked upon as a general trend only since there is only one point for Mach numbers greater than 3. That one point is also placed on the graph with some amount of uncertainty about its exact location since the temperature recovery factor at Mach 0 for this data was not available and had to be assumed as one. The probe could have easily shifted in resistance between its oven and flow calibrations. Also, the data came from five different probes. Though each probe will show the same trend, they will have their own unique characteristics. In addition to the above findings, it is found that the temperature recovery factor is a function of the Reynolds number in the higher Mach number range ($M \geq 3$).

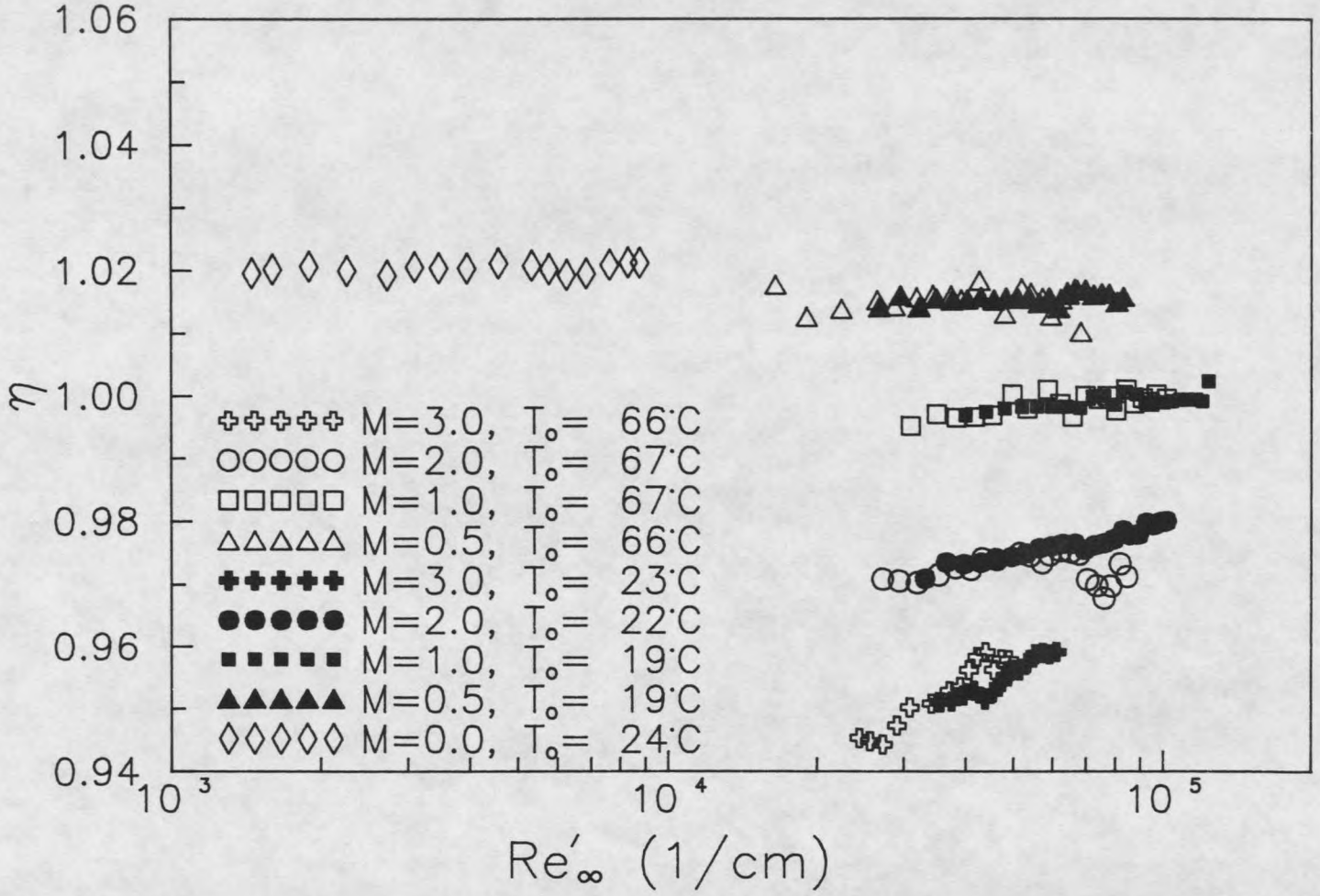

Figure 27. Temperature Recovery Factor Dependence on Flow Properties for Probe 48.

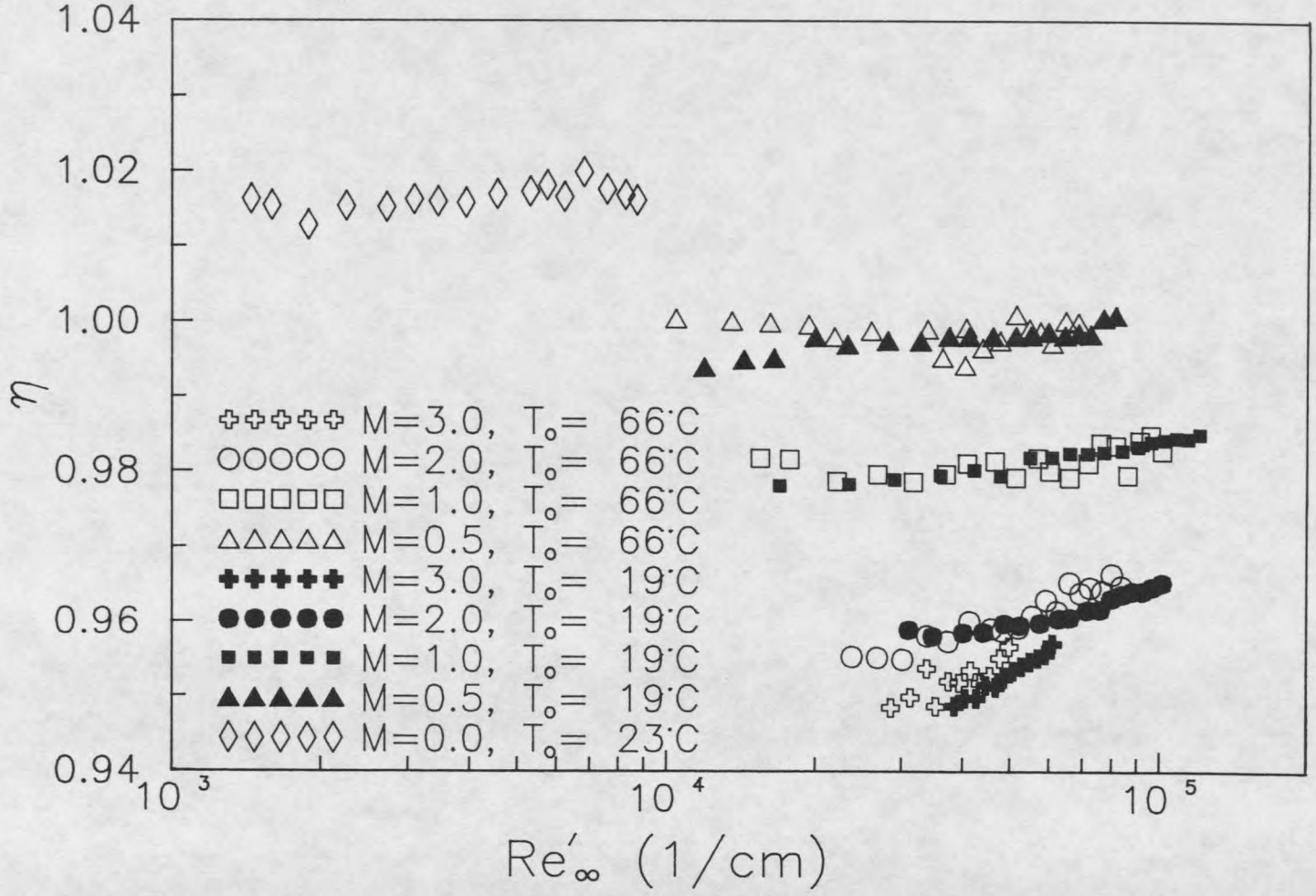

Figure 28. Temperature Recovery Factor Dependence on Flow Properties for Probe 50.

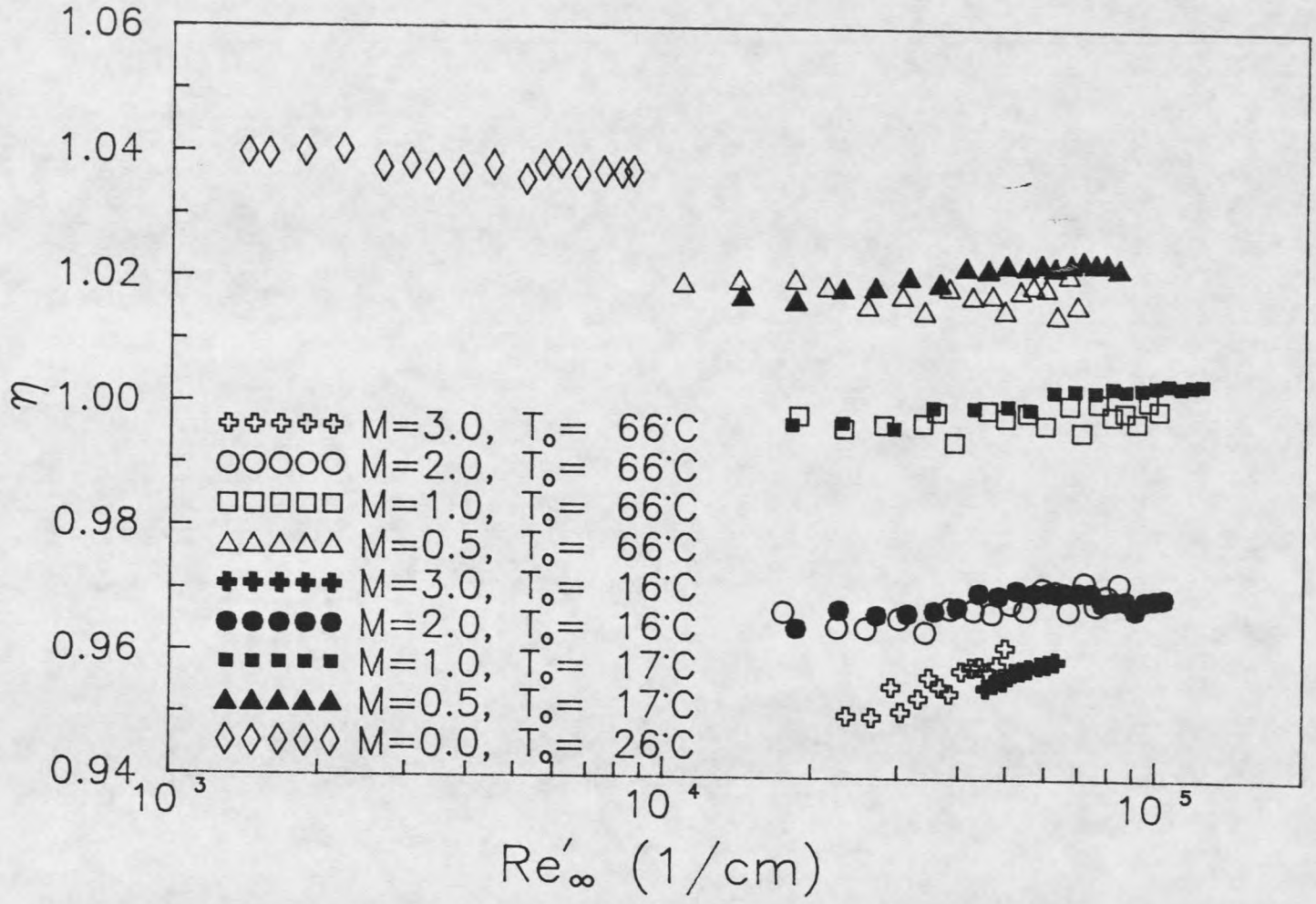

Figure 29. Temperature Recovery Factor Dependence on Flow Properties for Probe 56.

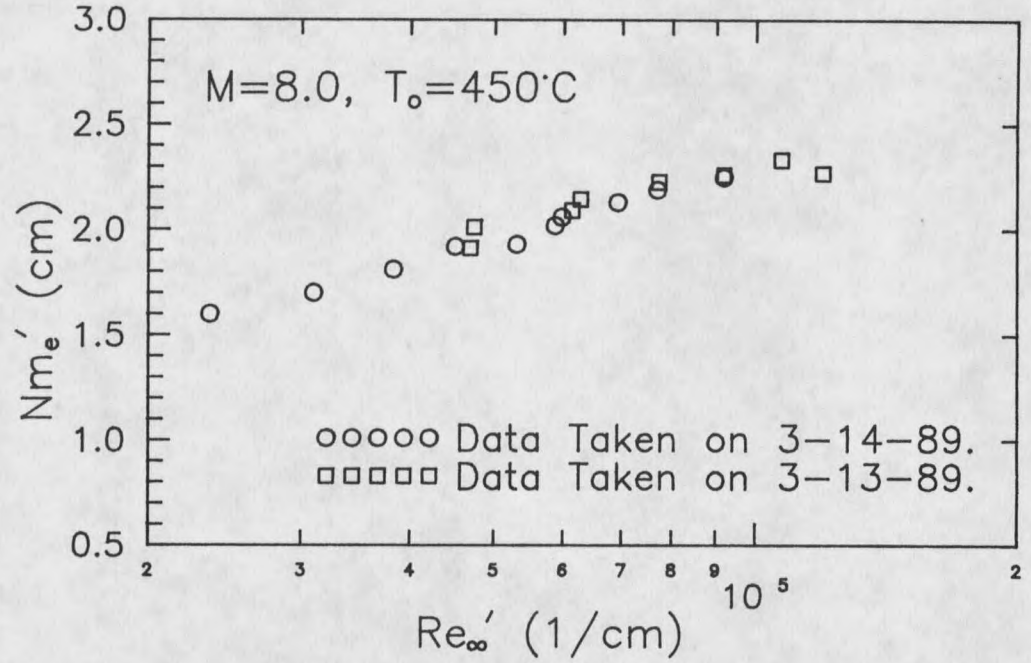

Figure 30. Measured Nusselt Number Characteristics in a Mach 8 Flow.

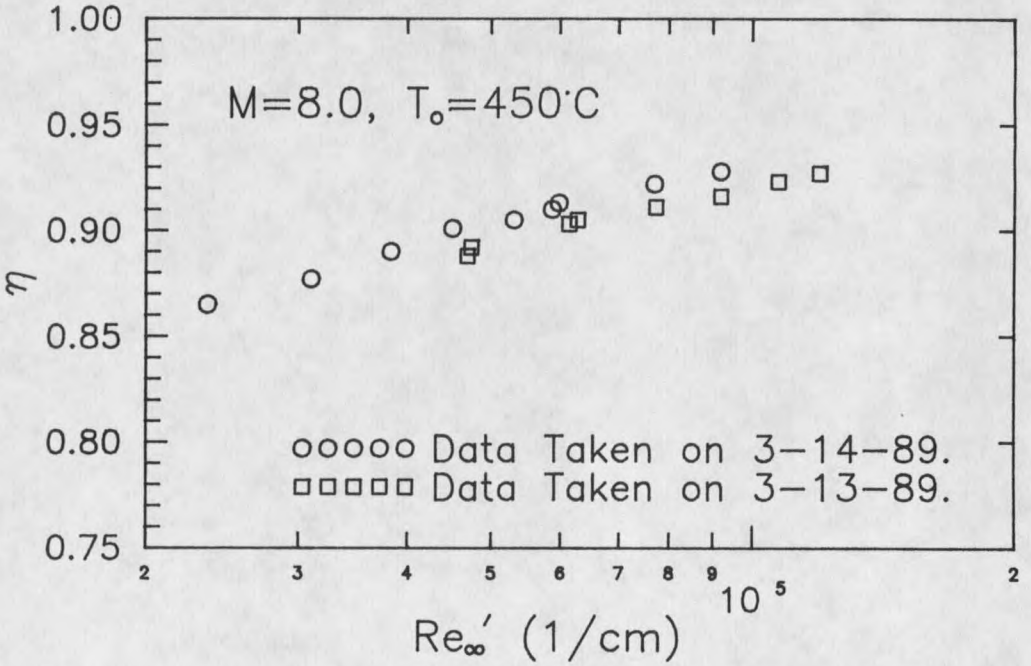

Figure 31. Temperature Recovery Factor Dependence in a Mach 8 Flow.

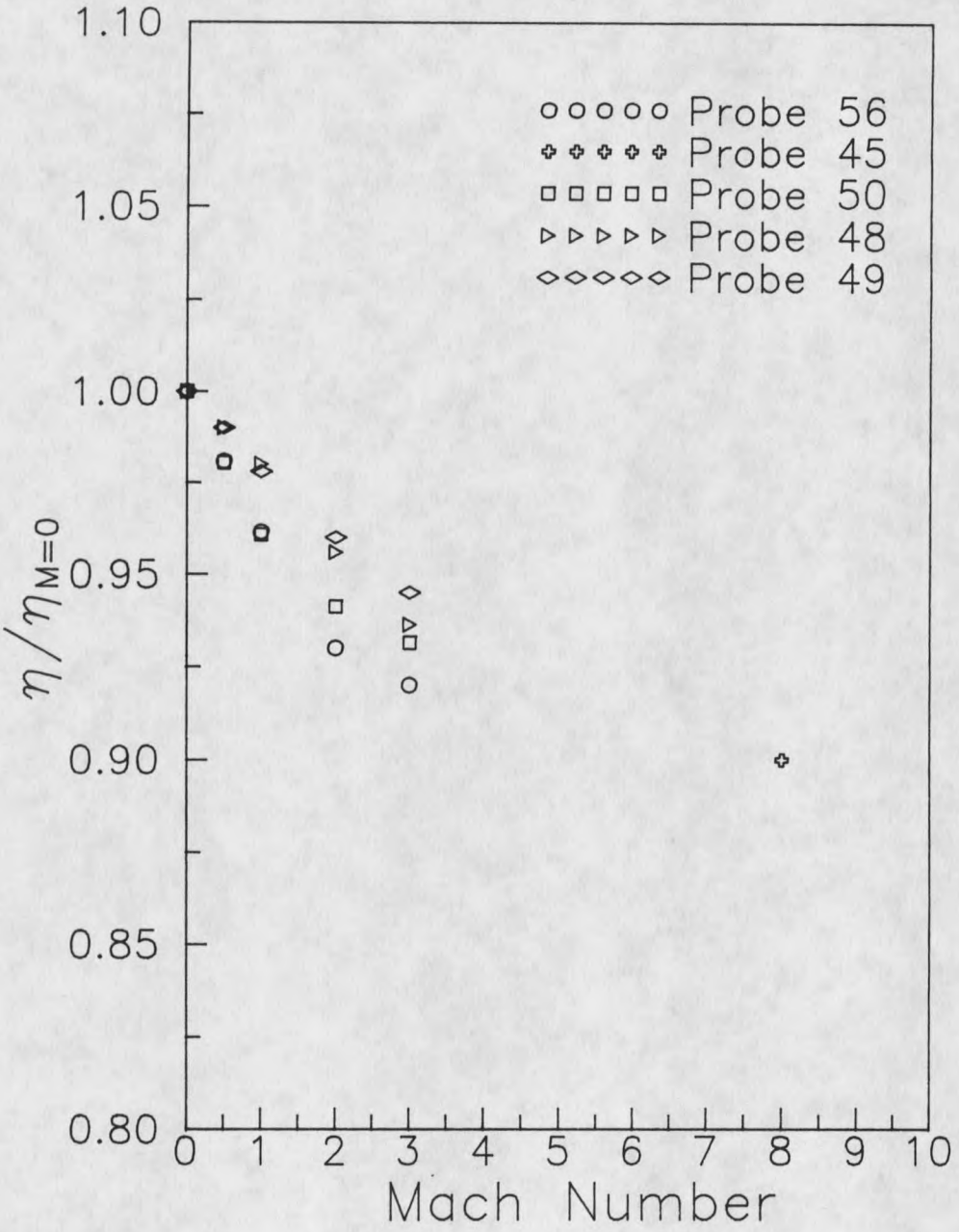

Figure 32. Normalized Temperature Recovery Factor Variation with Mach Number.

Nusselt Number Dependence On Flow Properties

The Nusselt number is found to be a more complicated function and even more complicated to obtain. By the method described in Chapter 4, the Nusselt number can be determined as a function of the flow properties. The results of the measured Nusselt number versus dimensional Reynolds number are shown in Figures 30, 33, 34, and 35. According to Kings Law the data should plot as a straight line, which they do, if plotted against the square root of the Reynolds number as is done in Figures 36, 37, and 38. Notice that the measured Nusselt number, which contains conduction and convection effects, is a function of Reynolds number, stagnation temperature, and Mach number. However, this measured Nusselt number is not the variable of interest. The variable of interest is the "convective" or "actual" Nusselt number which can be obtained from the measured Nusselt number if it is corrected for conduction effects (refer to (28)).

It was estimated in Chapter 3 that the conduction contribution term should be a linear function of the form

$$\text{Ncnd} = c\sqrt{\frac{k_S}{k_e}} \quad . \tag{57}$$

As can be seen in Figure 39, this predicted linear dependence on the inverse square root of the thermal conductivity of the air surrounding the probe is quite good. This conduction contribution to the measured Nusselt number can more readily be used if it is plotted against the recovery temperature, as in Figure 40, since the recovery temperature is readily found. Knowing both the measured Nusselt number and the contribution to the measured Nusselt number by conduction, the "actual" unit Nusselt number can be determined. By simply subtracting the conduction contribution the "actual" Nusselt number is found. Typical results of this procedure are shown in Figures 41, 42, and 43.

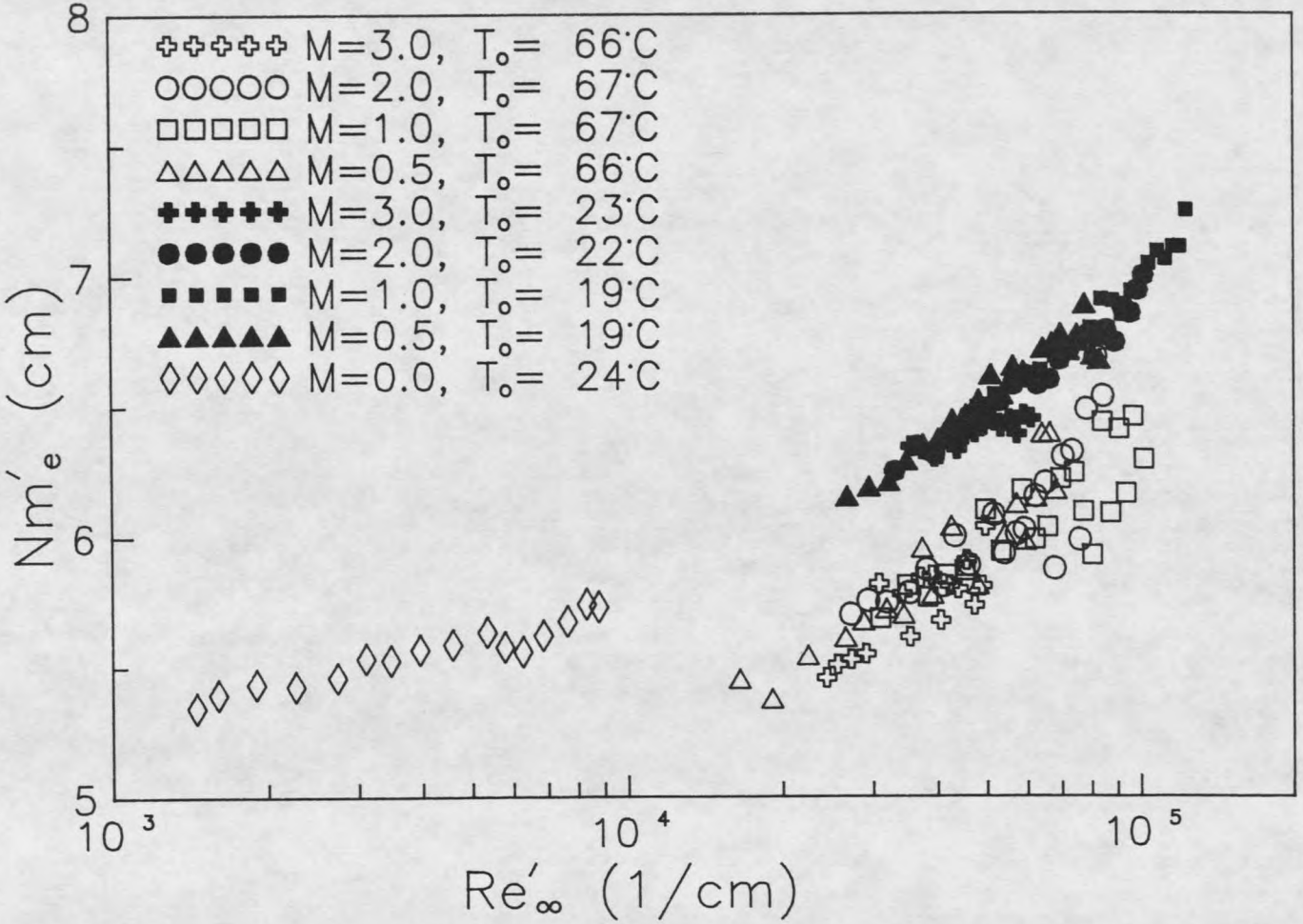

Figure 33. Measured Nusselt Number Characteristics for Probe 48.

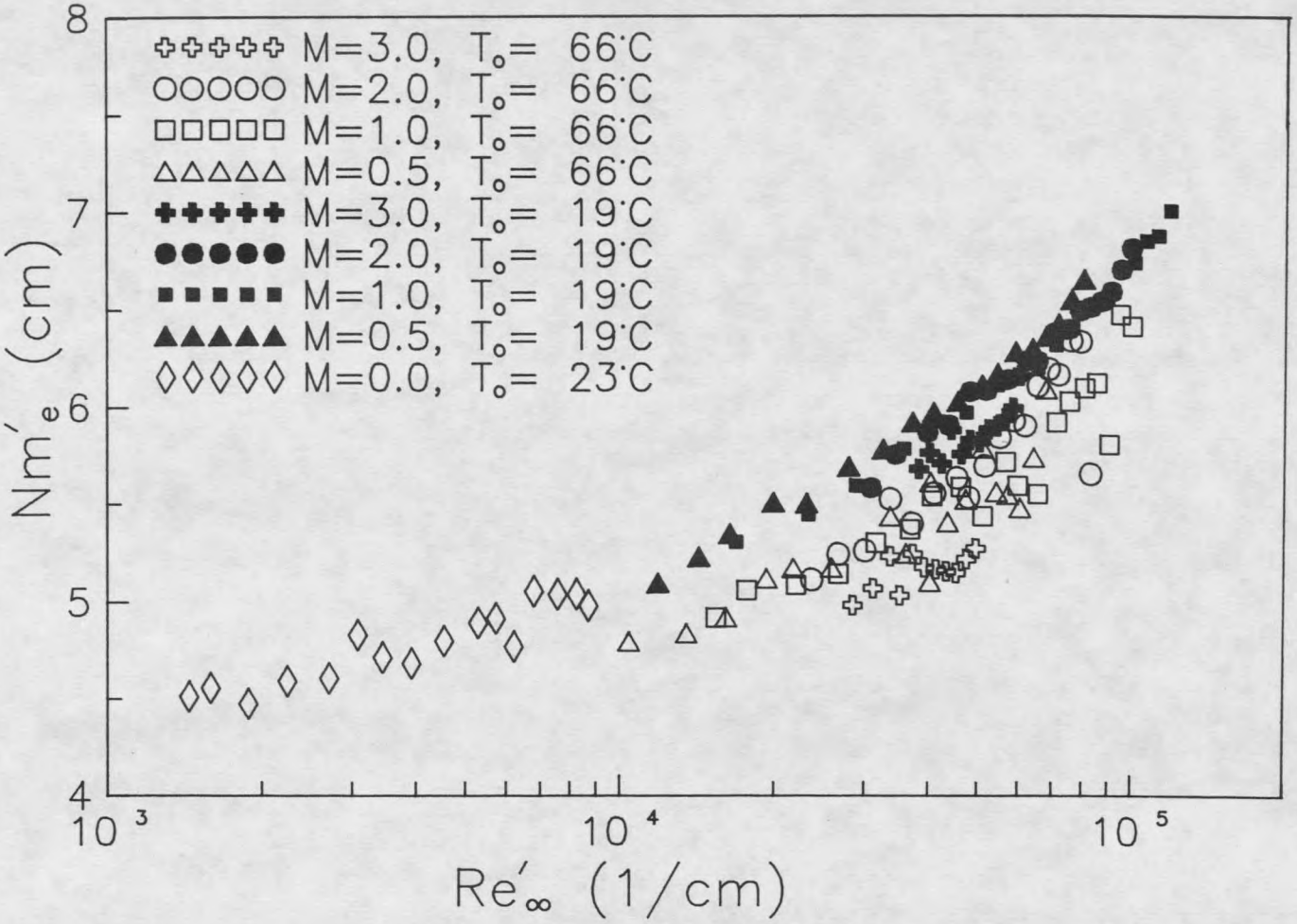

Figure 34. Measured Nusselt Number Characteristics for Probe 50.

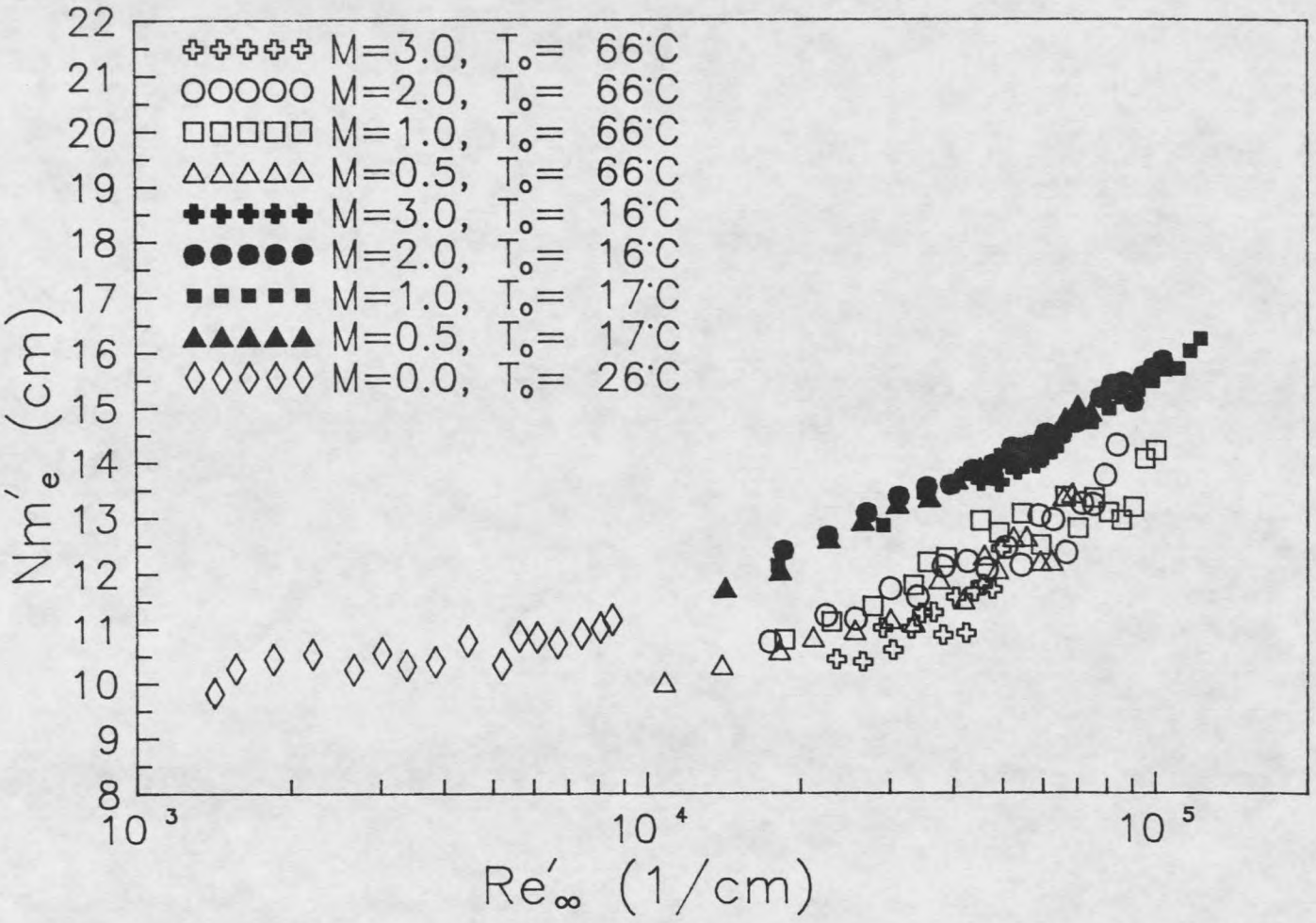

Figure 35. Measured Nusselt Number Characteristics for Probe 56.

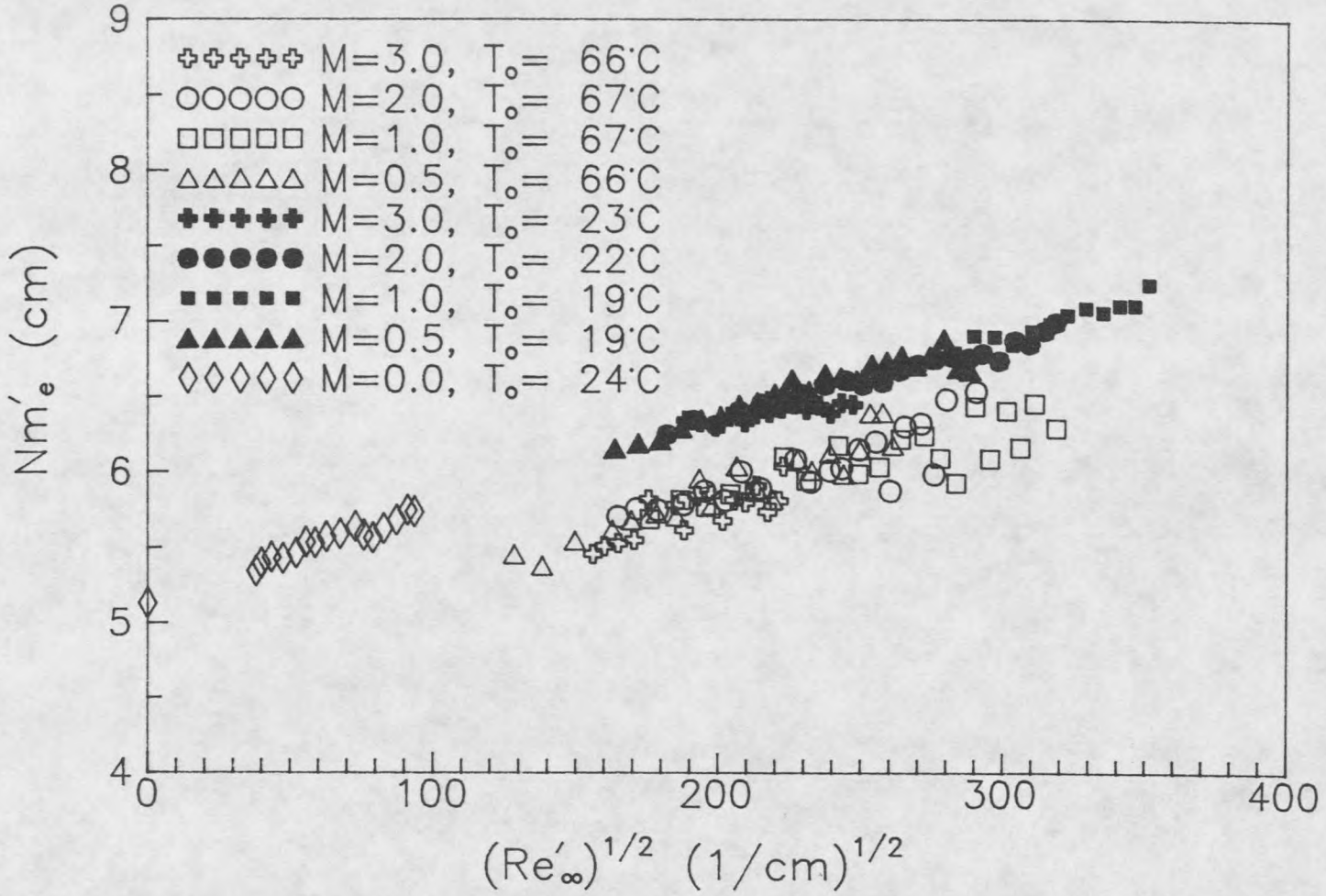

Figure 36. Measured Nusselt Number Characteristics for Probe 48 in Terms of the Square Root of the Reynolds Number.

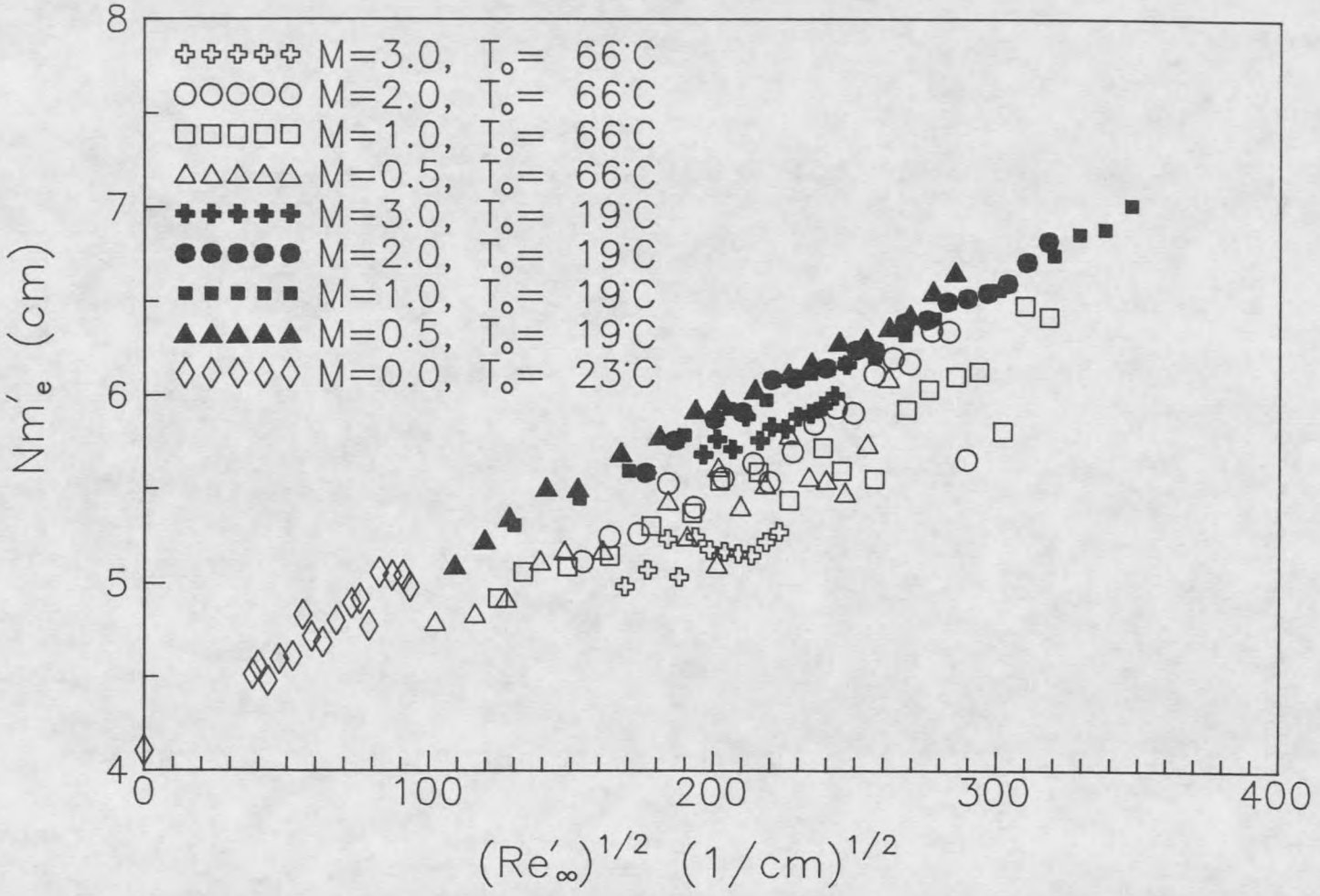

Figure 37. Measured Nusselt Number Characteristics for Probe 50 in Terms of the Square Root of the Reynolds Number.

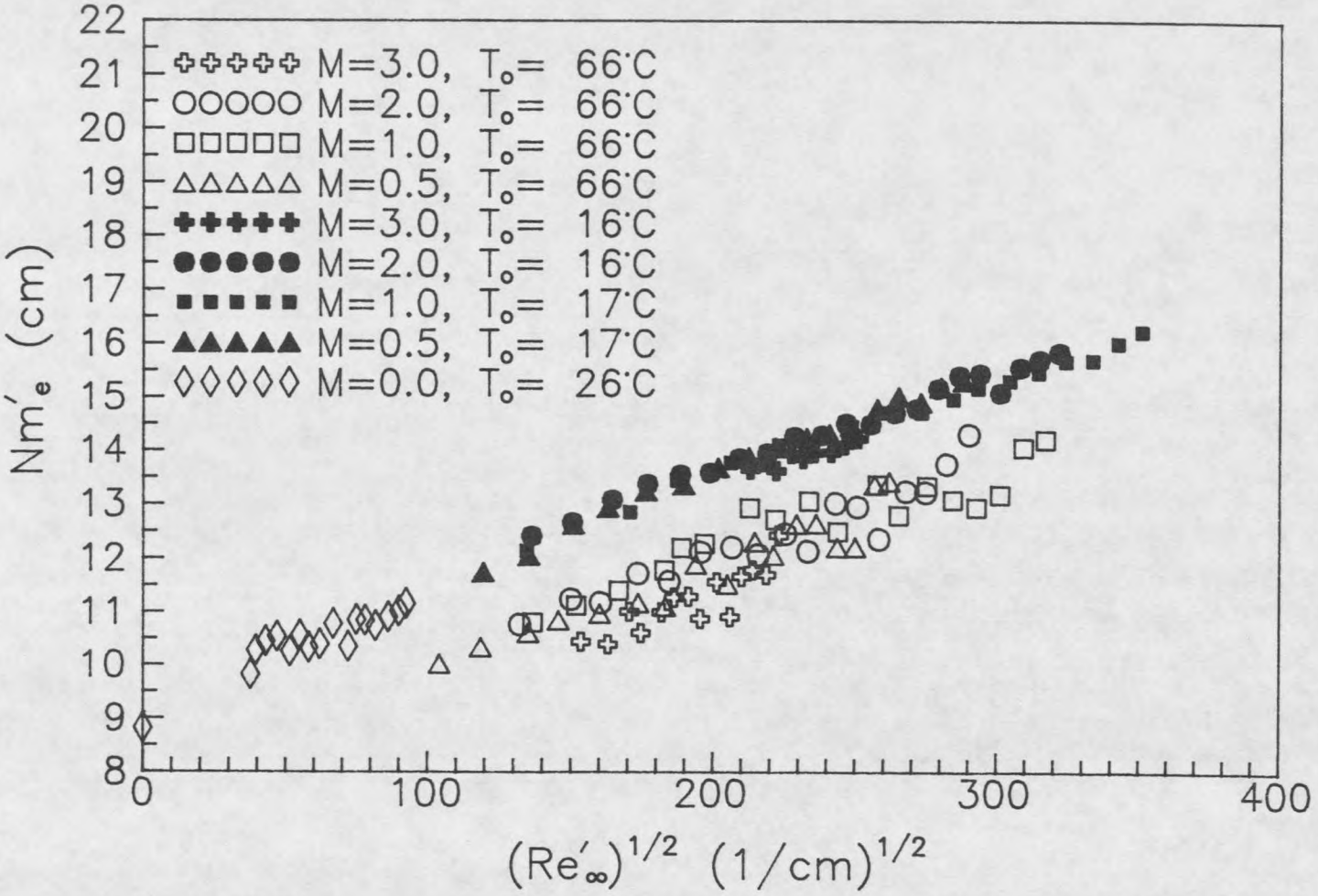

Figure 38. Measured Nusselt Number Characteristics for Probe 56 in Terms of the Square Root of the Reynolds Number.

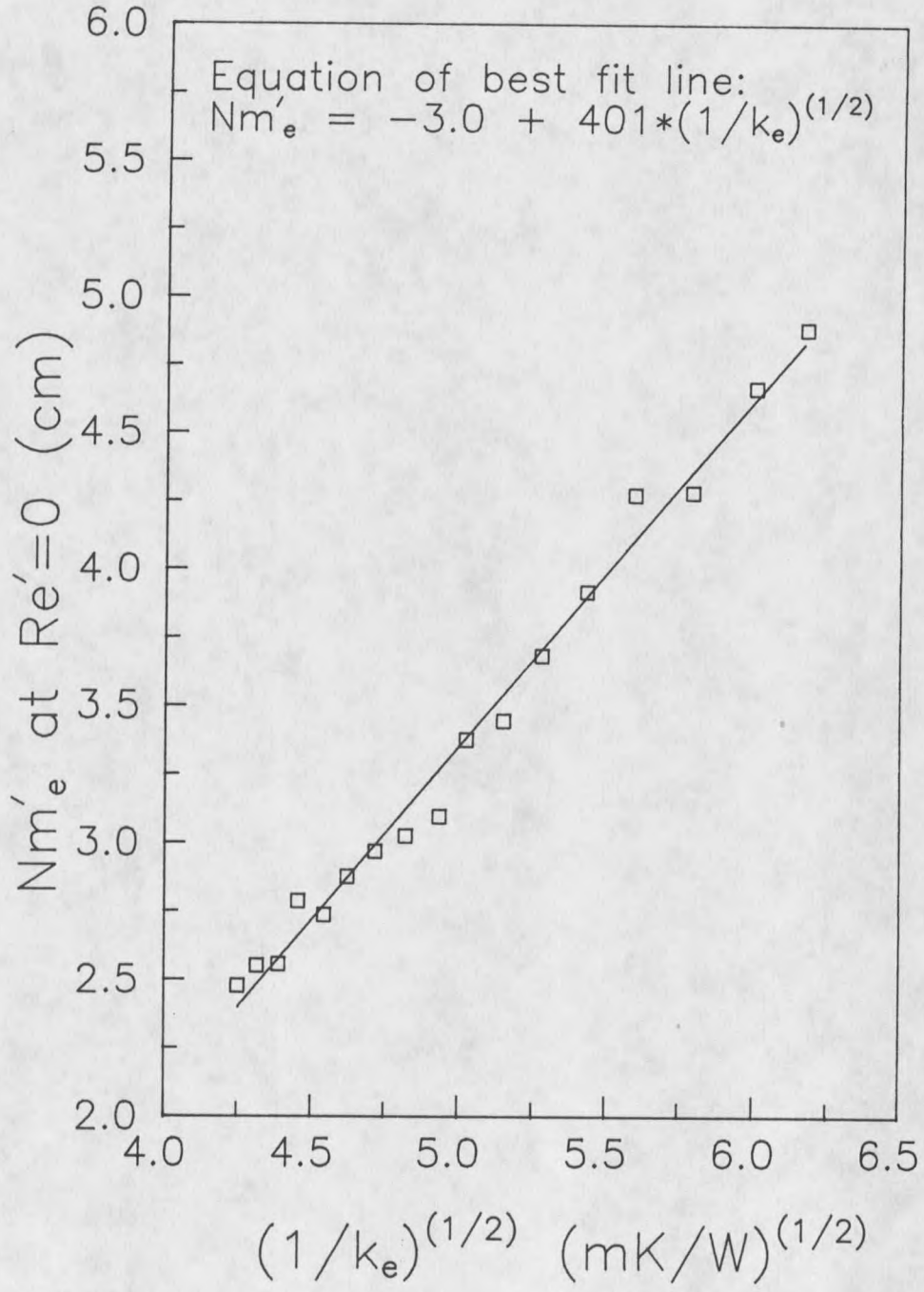

Figure 39. Measured Nusselt Number Dependence on the Inverse Square Root of the Thermal Conductivity in the Absence of Forced Convection.

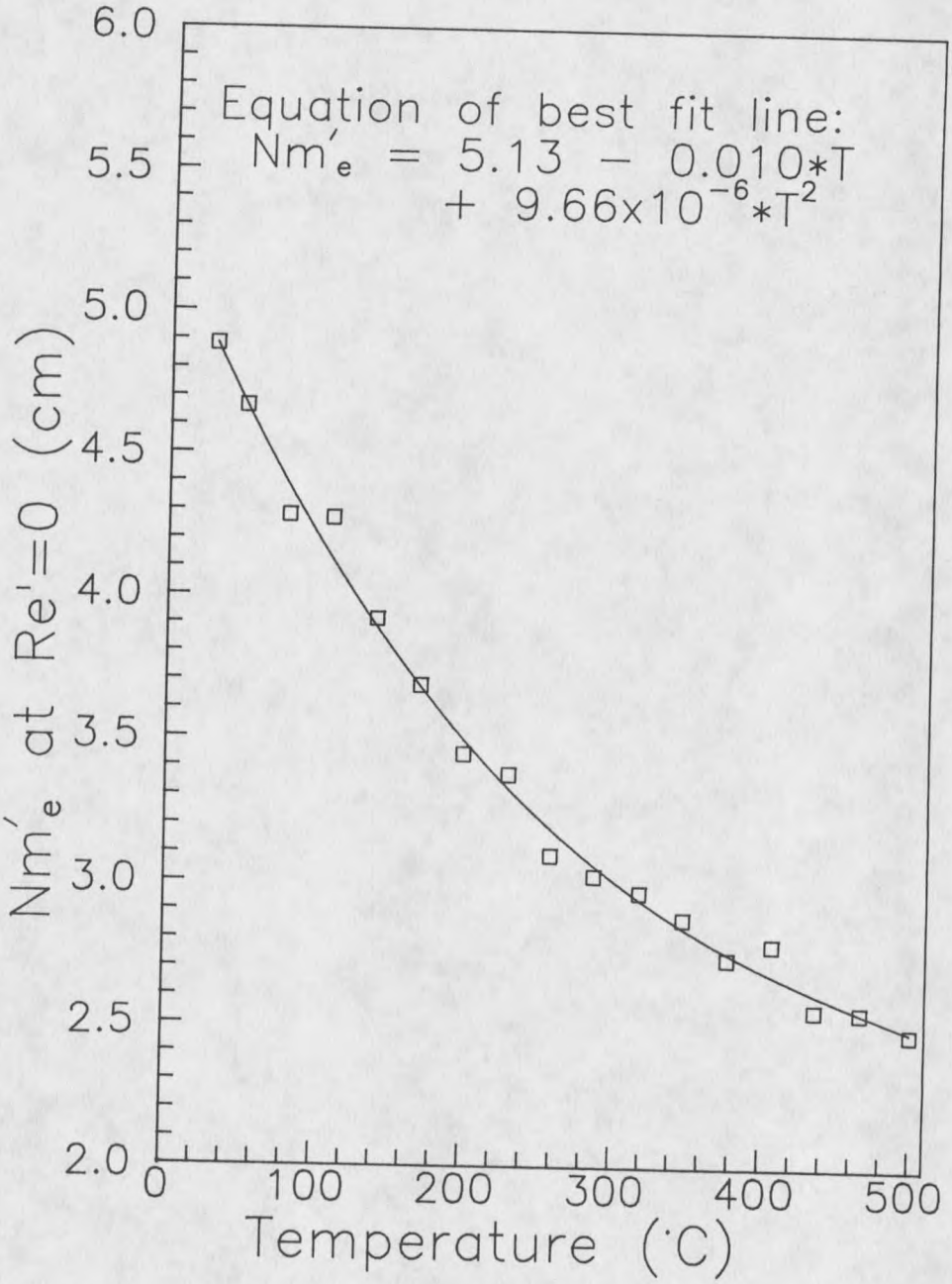

Figure 40. Temperature Dependence of the Measured Nusselt Number in the Absence of Forced Convection.

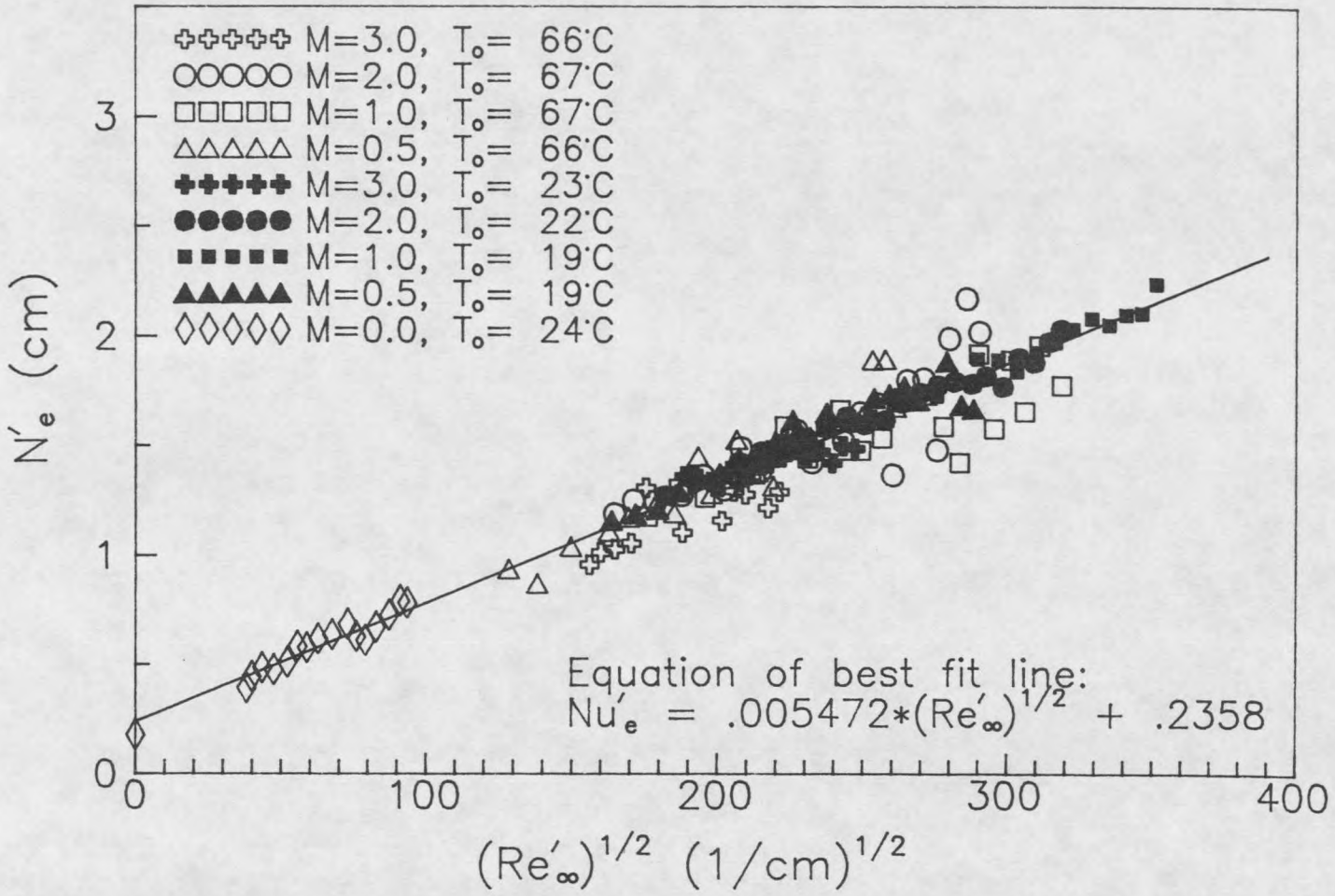

Figure 41. Convective Nusselt Number Characteristics for Probe 48.